Renewable Energy 101 (2017) 1–21

Contents lists available at ScienceDirect

Renewable Energy

journal homepage: www.elsevier.com/locate/renene

Assessing the European offshore wind and wave energy resource for combined exploitation

Christina Kalogeri [a], George Galanis [a, b], Christos Spyrou [a], Dimitris Diamantis [a], Foteini Baladima [a], Marika Koukoula [a], George Kallos [a, *]

[a] University of Athens, Department of Physics, Atmospheric Modeling and Weather Forecasting Group, University Campus, Bldg. PHYS-V, Athens 15784, Greece

[b] Hellenic Naval Academy, Section of Mathematics, Mathematical Modeling and Applications Laboratory, Hatzikiriakion, Piraeus 18539, Greece

ARTICLE INFO

Article history:
Received 10 February 2016
Received in revised form
25 July 2016
Accepted 5 August 2016

Keywords:
Offshore wind energy
Wave energy
Deep offshore
Combined exploitation

ABSTRACT

The main concern when utilizing renewable energy resources is their intermittency and variability. One way to deal with this shortcoming is to harvest energy from complementary sources. In this study, wind and wave energy were selected as such and further analyzed in terms of availability, variability, coherence, correlation and potential impact from extreme values. This resource characterization was performed in different timescales, during a 10-year period, using high resolution numerical modeling systems. Based on the results of this analysis, the most suitable areas for combined exploitation were identified and the possible merits from this synergy were pin-pointed and discussed. It was indicated that the most suitable areas for combined use are the western offshore areas of Europe. The wind and wave fields in these open sea areas reveal the lowest correlation in the examined field in contrast to those located in semi-enclosed and enclosed basins that exhibit the highest ones. The joint exploitation in the former regions gives a less variable power output with considerable fewer hours of zero production. Moreover, the suitable energy conversion system for a specific area is strongly dependent on the local characteristics of the available resource.

1. Introduction

Europe has the leading role in the marine power utilization. It accounts for more than 90% of the world's installed offshore wind capacity, while setting targets to cover the 4% of the electrical demand until 2020. The near-shore (less than 50 m) wind power capacity has already reached GWs levels. As the demand for renewables is rising, suitable near-shore sites become sparse, driving the technology to go to higher depths (>50 m). Moreover, deep sea areas like the Mediterranean Sea, the Norwegian coasts or the Atlantic coasts of Europe are experiencing high offshore wind resource that cannot be exploited by the current technology. New offshore designs are to be developed to harness the large wind power potential of the deep offshore environment. For this reason, industry is moving from fixed foundations to floating substructure technology, following the standards of the mature oil and gas industry. However, deep offshore technology is at an early stage of development, facing great challenges especially due to the high design, installation and maintenance expenses.

To compensate with such high costs, potential synergies among complementary resources can provide suitable solutions. In particular, joint exploitation of offshore wind and wave energy is able to increase the energy yield per square meter and at the same time to reduce the variability and the hours of zero production, in areas where the two resources have low correlation. Furthermore, it can lower the operational and maintenance costs, since the two will share common installations [1,2]. Considering now an efficient layout of wave energy converters (WEC's) inside a wind farm, the local wave climate will be modified, providing a sheltered environment for operation and maintenance. The latter can enlarge the accessibility weather windows and protect the wind turbines (WT) from heavy wave loads during storm conditions [3].

In order to optimally harvest the power from wind and waves there is a need for detailed resource characterization that takes into consideration the diversity of the two resources. A number of studies have assessed the wind and wave power potential, independently, either globally [4,5] or at specific sites [6,7]. Several authors used measurements, in-situ or satellite data, solely or along

* Corresponding author.
E-mail address: kallos@mg.uoa.gr (G. Kallos).

http://dx.doi.org/10.1016/j.renene.2016.08.010
0960-1481/

with numerical model outputs [8–12] while others utilized only the results from numerical models for the same purpose [13–15]. Furthermore, data from large hindcast projects performed by well-known operational centers like ECMWF, NCEP etc. have been also widely used to perform such kind of analysis [16–20]. These datasets have the advantage of a wide spatial and long temporal coverage and the disadvantage of a rather coarse resolution. Despite the latter they have been proven useful basically for providing the basis for statistical [21] or dynamical downscaling [7,22–24].

When it comes to combined resource analysis little has been done. Combined exploitation is a rather recent topic and thus few studies have been performed. The vast majority of them worked on a joint wind/wave power analysis at specific locations, either at test sites or at locations where measurements were available [1,3,25–28]. However, most of the research toward this direction has been performed in the framework of EU funded projects that aimed to identify possible synergies for deep offshore resource exploitation [29–34].

In this study, an attempt was made to perform such kind of analysis for the entire offshore area of Europe, using a high resolution wind and wave dataset. More specifically the MARINA database was used [30,31]. This database has been produced in the framework of the MARINA Platform project, using the results of atmospheric/wave modeling hindcast simulations, for a period of ten years (2001–2010). It provides co-located, high resolution information for the main met-ocean parameters and thus was selected for the combined resource characterization. It has been previously used and evaluated for its accuracy, in several studies [2,35–38]. In this work further analysis is performed and the main objectives are:

- To identify the main features of the available offshore wind and wave energy resource of Europe.
- Based on these, to result in favorable locations for combined energy exploitation.
- To evaluate the possible benefits of the combined exploitation on the final power output, in terms of availability and variability.

This paper is organized in the following five sections. In Section 2 a short description of the main climatological characteristics of the offshore areas of Europe is presented. The methodology adopted for the assessment of the wind and wave power resource is presented in Section 3 and the main results of the analysis are presented in Section 4. Finally in Section 5 a brief discussion summarizes the main findings.

2. Study area and prevailing weather patterns

This study is focused on the resource characterization of the deep offshore areas of Europe. The region can be divided in three sub-areas: The North and Baltic Sea, the European coastline that is exposed to the Atlantic Ocean and finally the Mediterranean and the Black Sea. These areas reveal different physiographic and weather characteristics that influence the renewable resources.

Europe is located in the mid-latitudes and thus is characterized by intense atmospheric activity. The western offshore areas of Europe are exposed to the Atlantic Ocean. These areas are strongly influenced by the extra and in some occasions post-tropical cyclones and polar lows that are generated along the Polar and the Arctic front respectively. Their transition paths are strongly controlled by the phase of the North Atlantic dipole (Azores high and the Icelandic low), following the paths of the prevailing westerlies. The intense storm activity over the Ocean creates strong swells that travel hundreds of kilometers towards the western European coasts, controlling the wave climate of the area [19,39,40].

The northern regions of Europe are bounded by the North and the Baltic Sea. The wind and wave conditions in these semi-enclosed, shallow water basins are also controlled by the passage of cyclonic systems such as extra-tropical cyclones and on some occasion polar lows. Strong cyclonic activity is revealed during the positive phase of the North Atlantic oscillation (NAO) (strong Icelandic low and strong Azores high) that enhances and shifts the westerly zonal flow and the cyclones towards the area. The sea wave conditions for both the Baltic and the North Sea can be considered as wind-driven due the limited fetch of the basin.

The closed, deep water, Mediterranean Sea is the southernmost bound of Europe. It is surrounded by complex mountainous terrain and is divided in several sub-basins with different characteristics (Tyrrhenian, Aegean, Ionian, Adriatic and Levantine Sea). The narrow passages between the mountainous ridges channel the air masses toward the Mediterranean. The weather in the area is also affected by the mid-latitude cyclones that reach the basin especially during the negative phase of the NAO (weak Icelandic low and weak Azores high). Nonetheless, the large majority of cyclones are generated within. They differ from the North Atlantic systems in scale, intensity and duration. The spatial distribution of cyclones reveals a seasonal behavior. The complex terrain of the coastline, the high Sea Surface Temperature (SST) along with the high land surface temperature of the northern coastal areas of Africa form a highly baroclinic region, that provides favoring conditions for the generation of cyclones [41–44]. The main cyclogenetic areas are the Gulf of Genoa, the lee side of the Atlas Mountain and the area near Cyprus. Moreover, the Aegean Sea, the Ionian Sea, the Gulf of Syrtis, the Iberian Peninsula and the sea area of Algeria can be considered as secondary cyclogenetic areas.

3. Methodology

To identify suitable locations for the joint exploitation of wind and wave energy resource and to further evaluate the impact of this combined use on the variability of the final aggregate output, a detailed resource and site assessment was performed over the offshore areas of Europe.

In particular, the two energy resources were analyzed in terms of availability, variability, potential impact from extremes, coherence and correlation. The availability, the coherence and the variability were assessed based on the mean and standard deviation values. These were further quantified and evaluated regarding the spatiotemporal variability in seasonal and yearly scales. The possible impact from extremes was estimated, during the decade, using the higher moments of the dataset, namely skewness and kurtosis. The latter give information about the symmetry of the dataset and the infrequent extreme deviations from the mean.

The data used for the aforementioned analysis are the product of hindcast numerical simulations. This dataset was produced in the framework of the FP7 MARINA Platform project [30,31] and provides information for the main met-ocean parameters needed for a detailed resource assessment.

3.1. MARINA platform database

The hindcast dataset used for this study provides information for the entire European coastline, for the period between 2001 and 2010, with an hourly time frequency and a spatial resolution of 5 km (Fig. 1). The modeling system used to construct the dataset consists of the limited area atmospheric model SKIRON [45–47] and the 3rd generation wave model WAM [48,49]. The atmospheric/wave modeling system has been utilized and evaluated in a

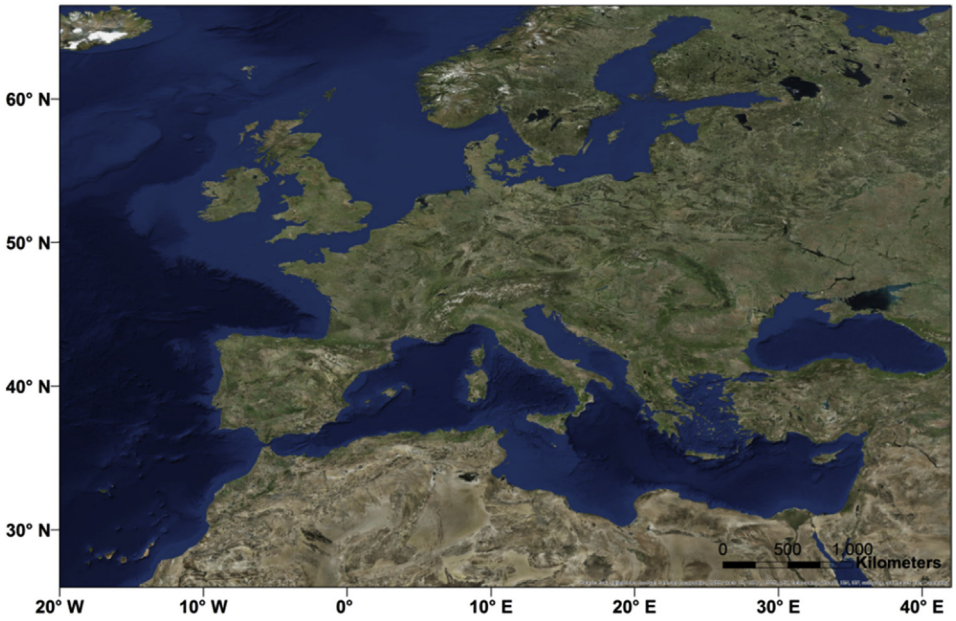

Fig. 1. Study area.

number of major European projects such as: Marine Renewable Integrated Application (MARINA Platform), MFSTEP, ANEMOS, ANEMOS+, IRPWIND, ENVIWAVE, POWWOW, ADIOS, MEDSEA and so on (see for details: http://forecast.uoa.gr/oldproj.php) and in numerous research, technical and operational studies [15,47,50–53].

The system has assimilated available surface and upper air observations from the global network through advanced assimilation schemes [54,55]. In particular, the atmospheric model assimilated data from the global rawinsonde observation program (Raob), METARS and surface synoptic observations (SYNOP). The wave model assimilated altimeter significant wave height, H_s, data from ENVISAT. The main characteristics and the configuration of the models are presented in Tables 1 and 2.

The model outputs used for the offshore wind resource analysis are the wind speed and the air density at 80 m. This height was selected as representative for offshore wind energy applications. For the wave energy resource the integrated products of the directional wave energy spectrum $S(f,\theta)$, significant wave height, H_s, and energy period, T_e, were utilized. The latter are calculated by means of spectral moments m_n as follows:

$$m_n = \int_0^{2\pi}\int_0^{\infty} f^n S(f,\theta) df d\theta \quad n = -1, 0, 1, 2 \tag{1}$$

where f represents the frequency and θ the direction.

Table 1
Configuration of the atmospheric model (SKIRON).

SKIRON	
Resolution	0.05°
Vertical levels	45 (up to 20 km) – step mountain coordinates
Time-step	12s
Initial conditions:	0.15° reanalysis fields from LAPS [54,55]
Boundary conditions:	0.15° reanalysis fields from LAPS (every 3 h)
24-category USGS (30-sec) land use/land cover system [56]	
16-category soil characteristics dataset [57]	
Daily SST fields from NCEP with 0.5° resolution	

$$H_s = 4\sqrt{m_0}, \quad T_e = m_{-1}/m_0 \tag{2}$$

3.2. Intercomparison between hindcasted data and observations

For this analysis the hindcast data have been compared with available buoy measurements at several offshore areas (60 buoys and two offshore masts in the North Sea). The buoy data were retrieved from the EMODnet portal [58]. In particular, the available 10 m wind speed from 27 buoys has been compared with the 10 m wind speed derived by the atmospheric model. On the other hand, the H_s measured by 60 buoys, was compared against the wave model results. The areas covered are: the western coasts of Europe, the English Channel, the Aegean, the Ionian and the Baltic Sea. Regarding the H_s the available data have a wider spatial coverage (60 buoy sites) and longer records. It is important to note that all the selected data have not been used during the assimilation procedure and thus they can be considered as independent sources. More information regarding the location, the duration and the number of data used can be found in Appendix 6.1 (Fig. 20 and Tables 7–8).

The statistical indices selected to assess the spatiotemporal behavior of the parameters are: The Bias that gives an estimation of the mean error, the Correlation Coefficient (R), the RMSE, the Standard Deviation (σ) and the Scatter Index (SI). The latter is expressed as the ratio of RMSE to the mean [59]. It has to be noted that the RMSE and the R are sensitive to large differences between modeled and observed values and also to outliers. Moreover, they can be easily affected by small phase errors [60]. In any case we decided to derive multiple indexes in order to extract solid conclusions.

The correlation between measured and simulated 10 m wind speed is higher than 0.7 in the vast majority of the sites. This behavior indicates a usual performance of a mesoscale model for the selected resolution [61–64] (Fig. 2a). Similar satisfactory behavior is evident also for H_s. For the vast majority of the buoy sites the R values of H_s are higher than 0.8 while for most of the Atlantic facing coasts is even higher than 0.9 (Fig. 2b).

Table 2
Configuration of the wave model (WAM).

WAM (Cy33r1)	Resolution	Frequencies	Directions	Time-step	Wind forcing
North Atlantic	0.05°	25 (0.0417–0.5476 Hz) Logarithmically spaced	24 equally spaced	75s	10 m winds SKIRON Every 3-h
Mediterranean – Black Sea	0.05°	25 (0.0417–0.5476 Hz) Logarithmically spaced	24 equally spaced	45s	10 m winds SKIRON Every 3-h

Bathymetry: ETOPO1 1arc-minute.

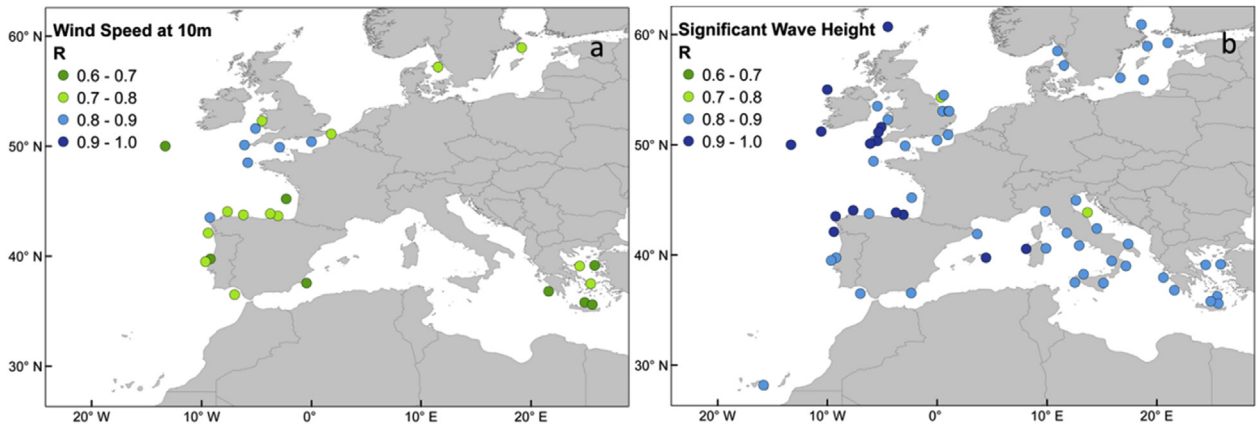

Fig. 2. Spatial distribution of the correlation coefficient (R) of a) wind speed at 10 m and b) significant wave height.

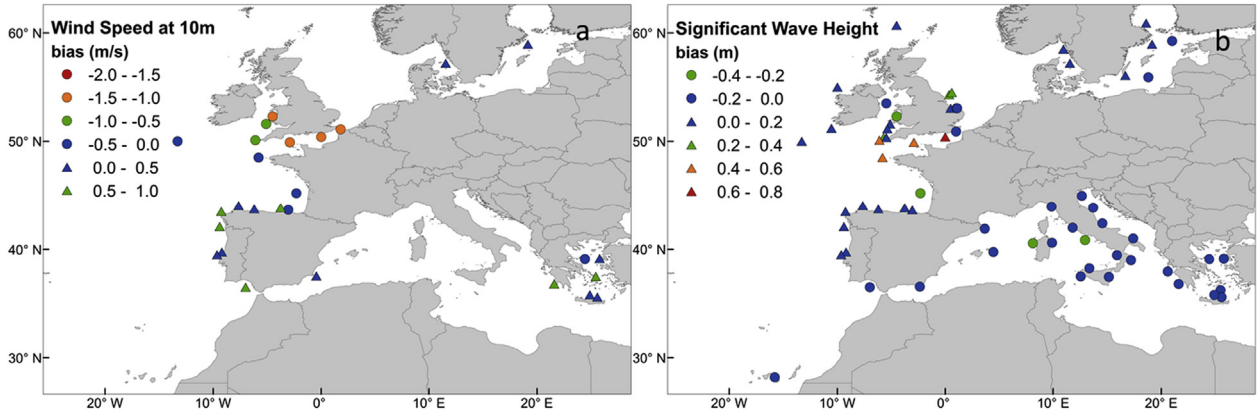

Fig. 3. Spatial distribution of the Bias of a) wind speed at 10 m and b) significant wave height.

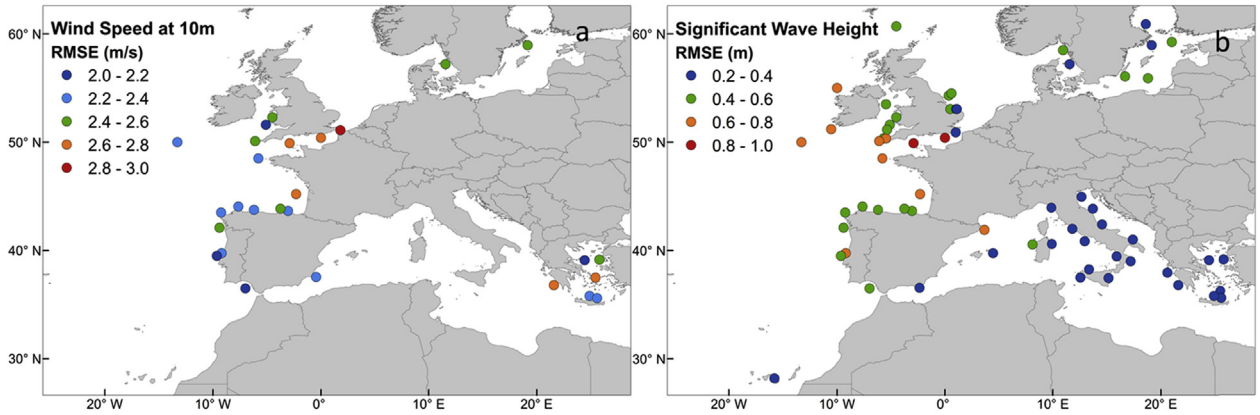

Fig. 4. Spatial distribution of the RMSE of a) wind speed at 10 m and b) significant wave height.

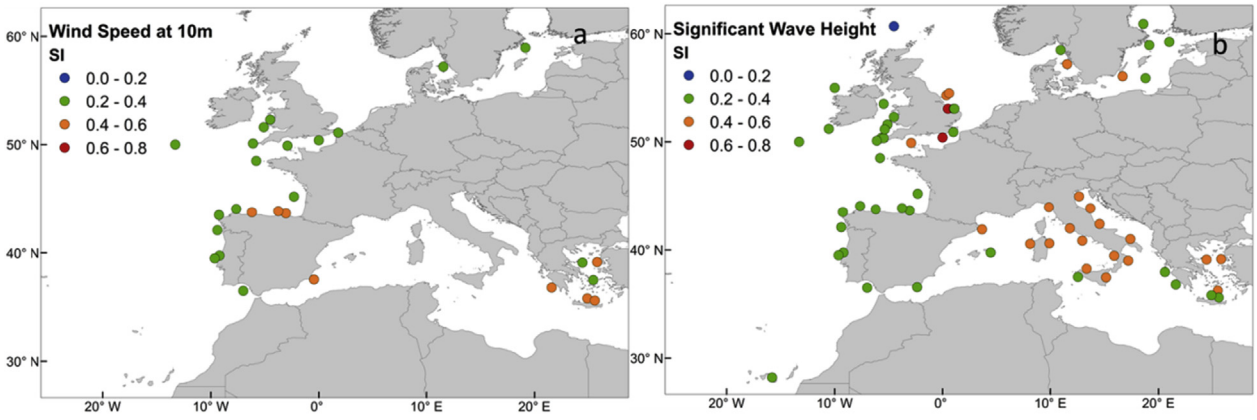

Fig. 5. Spatial distribution of the scatter index (SI) of a) wind speed at 10 m and b) significant wave height.

The Bias for both 10 m wind speed and H_s is rather small over the whole domain as illustrated in Fig. 3. In particular for the 10 m wind speed the Bias ranges between ±1 m/s, while for H_s between −0.4 m and 0.2 m as can be seen in Fig. 3a and b respectively. The English Channel seems to have the highest values of systematic error both for winds and waves (Fig. 3). In the areas located off the Iberian Peninsula both 10 m winds and H_s are slightly overestimated (Fig. 3). The opposite is the case for the Gulf of Biscay as shown in Fig. 3. The H_s in the Mediterranean Sea is slightly underestimated exhibiting Bias values of no more than 0.4 m (Fig. 3b). In the Celtic Sea, the Aegean Sea, the Ionian Sea and the straits of Gibraltar the 10 m wind speed and the H_s are slightly overestimated (Fig. 3). Systematic error can be considered as the most important statistical measure for the overall estimation of the power resource.

The RMSE of the 10 m wind speed, in almost all cases apart from the English Channel and some buoy locations in the Aegean Sea and the Bay of Biscay, is less than 2.6 m/s (Fig. 4a). Rather low values,

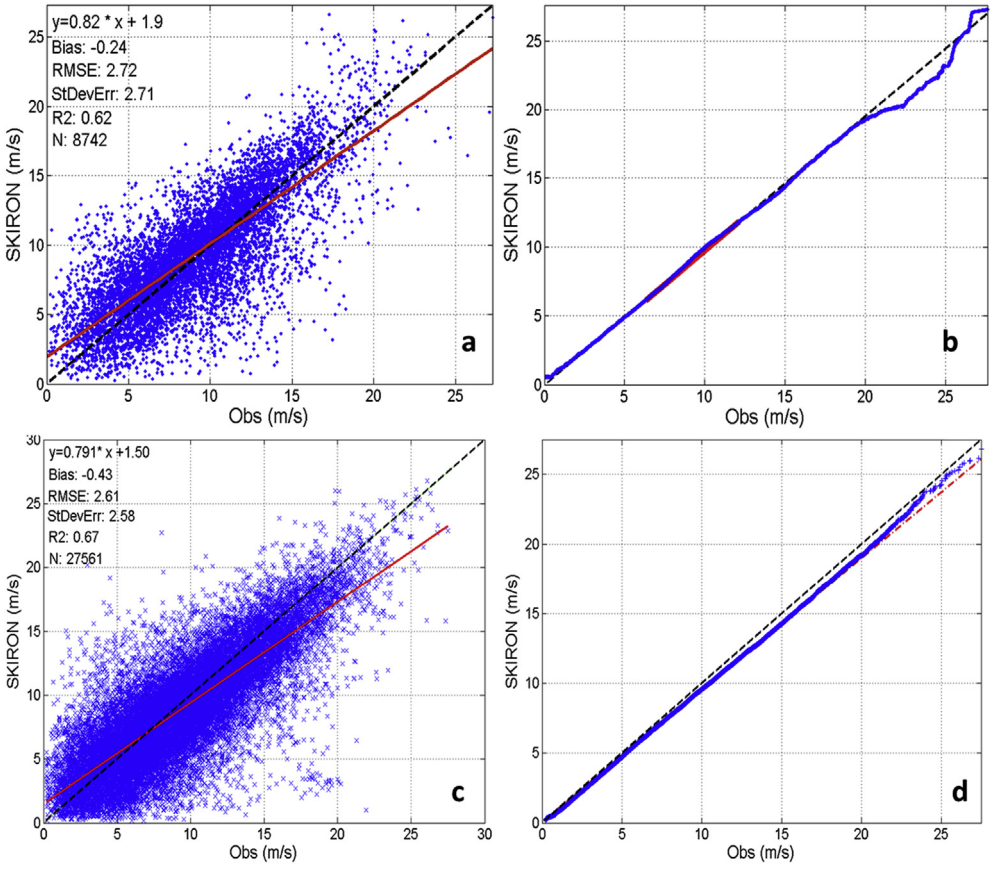

Fig. 6. Comparison between (a) modeled (SKIRON: 54.00N 6.60E) and observed (FINO1: 54.01N 6.58E) wind speed at 80 m and between (b) modeled (SKIRON: 54.00N 6.60E) and observed (FINO1: 54.01N 6.58E) quantiles of wind speed at 80 m, for the year 2009. Comparison between (c) modeled (SKIRON: 53.15N 0.75E) and observed (Docking Shoal wind farm: 53.16N 0.75E) wind speed at 80 m and between (d) modeled (SKIRON: 53.15N 0.75E) and observed (Docking Shoal wind farm) quantiles of wind speed at 80 m, for the years 2006–2009.

less than 0.8 m (except from two locations in the English Channel), is the case for H_s (Fig. 4b). Scatter index values between 0.4 and 0.6 for both wind and wave parameters show a quite satisfactory scatter of the data around the best-fit line (Fig. 5). The RMSE and the SI are associated with the existence of turbulence in the wind field and the ability of the model to resolve the high frequency perturbations [65]. It is well known that the high resolution models, despite the fact that they incorporate formulations to accurately resolve the small scale features they may mistime and misplace these [60].

To test the ability of the system to accurately depict the wind field in higher than 10 m levels, measurements from two offshore masts located at FINO1 (54.01°N 6.58°E - North Sea) and at the Docking Shoal wind farm (53.16°N 0.75°E) were used. From the available heights the 80 m was selected to be directly compared with the model's 80 m wind speed. The comparison was performed for the year 2009 for FINO1 and for the years 2006–2009 for the Docking Shoal wind farm. The 80 m is a typical height for offshore wind turbines. Regarding FINO 1, the scatter plot and the basic statistical indices used show that the model depicts the main wind field behavior (Fig. 6a). Though it seems that it underestimates wind speeds higher than 20 m/s as it is indicated through the quantile-quantile comparisons (Fig. 6b). However, for wind speeds lower than 20 m/s the model captured the overall energy of the system quite well. For the Docking Shoal wind farm mast, the scatter and the quantile-quantile plots, presented in Fig. 6c,d, show that the model performed well in all quantiles.

As resulted from the aforementioned statistical analysis, the main parameters characterizing the wind and wave fields are in a satisfactory agreement with the measurements. Thus, this dataset can be considered as reliable and can be used for further analysis in order to assess the wind and wave resources.

3.3. Offshore wind and wave power potential characterization

To estimate the available wind and wave power potential of the European offshore areas the following formulas were utilized:

- For the available wind power potential per unit of area (m^2) :

$$P_{wind} = \frac{1}{2}\rho U^3 \left(W/m^2\right) \tag{3}$$

where U is the wind speed at 80 m in (m/s) and ρ is the air density in (kg/m^3).

- For the omnidirectional wave power potential per unit width of wave front (m):

$$P_W = \left(\rho_w g^2/64\pi\right) H_s^2 T_e \cong 0.5 H_s^2 T_e \ (kW/m) \tag{4}$$

where ρ_w is the water density (an average value could be 1025 kg/m^3), g is the gravitational acceleration that is approximately 9.8 m/s^2. The wave power formula is valid under the deep water assumption.

In order to describe the spatiotemporal behavior of the wind and the wave fields, a statistical analysis was performed utilizing apart from the conventional mean value and the Coefficient of Variation (CV) expressed as the ratio of the standard deviation to the mean, two extra indices representing the higher moments of the dataset. These are the skewness that is a measure of the asymmetry of the probability distribution that describes the data

$$g_1 = N^{-1}\sum_{i=1}^{N}(x_i-\mu)^3/\sigma^3 \tag{5}$$

and the excess kurtosis that is a measure of its peakedness.

$$g_2 = N^{-1}\sum_{i=1}^{N}(x_i-\mu)^4/\sigma^4 - 3 \tag{6}$$

These two can be considered as indicators of the impact from extreme values.

4. Results

4.1. Wind and wave power resource characterization

Based on the main met-ocean parameters selected for the resource assessment (air density, wind speed at 80 m, H_s and T_e), the available wind and wave power density have been estimated. This analysis indicated that the windiest regions are located at high latitudes, with some exceptional hot spots in the Mediterranean Sea and the Canary Islands, as it can be seen in Fig. 7a. The mean H_s values seem to follow the spatial distribution of mean wind speed (Fig. 7b). Mean T_e has a more distinct behavior, separating the whole domain in two distinct areas: a) In open sea areas that are exposed to the long Atlantic fetch, with mean T_e values between 9 s and 10 s (swell dominated) and b) in semi-enclosed and closed basins considered as wind driven areas with mean periods of less than 6 s (Fig. 7c). For the latter the evolution of the wave field is strongly determined by the wind field while for the first is controlled by the remote generated swell.

In terms of availability and coherence, the highest wind and wave power resource exist in the NW offshore areas of Europe (latitudes >45°) and in the northern part of North Sea (Fig. 8). In these areas, the mean offshore wind power potential at 80 m exceeds the 600 W/m^2 while the mean wave power potential exceeds the 50 kW/m (Fig. 8). Areas of lower wind and wave power potential are located in the Bay of Biscay, off the coasts of Portugal and of the northern parts of Spain. Exception to the latter is the NW tip of the Iberian Peninsula that exhibits wind and wave power potential comparable to the most energetic northern sea areas of Europe. The southern part of the North Sea has an energetic wind climate but a rather weak wave power resource. Finally, the sea around the Canary Islands is also of increased interest, revealing considerable wind and wave power resource (Fig. 8).

The closed basins, such as the Mediterranean, the Black and the Baltic Sea, exhibit low wave power density values, less than 5 kW/m (Fig. 8). This is mainly due to the short fetching that does not let long period waves to be created. In these areas and especially in the Mediterranean, there are regions where the two resources experience low, but not negligible mean values. For the latter, favorable areas for combined exploitation are located in the Gulf of Lions, in the Sicily Straits (Central Mediterranean), off the coasts of Sardinia, off the NE coasts of the Balearic Islands (NW Mediterranean) and in specific sites in the Aegean Sea. The Gulf of Lions (NW Mediterranean) and the Aegean Sea (NE Mediterranean) can be alternatively considered as ideal areas for wind power exploitation since they reveal wind power potential comparable to the most energetic northern sea areas included the Baltic Sea (mean wind power potential ~500–800 W/m^2).

In terms of variability the Atlantic facing offshore areas of Europe have the lowest values, for both wind and wave energy resource, compared to the other regions. The variability was estimated using the CV index within the 10-year period. The open sea

areas exhibit lower variability than the closed and semi-enclosed basins as illustrated in Fig. 9.

It is worth mentioning, that in closed basins the wave power is more variable than the wind power, as estimated by the 10-year analysis. This is typical for areas where the energy potential, in our case the wave energy, exhibits low mean values (<10 kW/m) and at the same time is influenced by frequent storm events. The latter can be considered as extremes and are responsible for the deviation from the central tendency (Fig. 9b). Increased variability compared to the other western coastal areas of Europe has the Bay of Biscay. This is the case for coastal areas bounded by land with complex topography that interferes with the prevailing wind direction. Such areas are the SW coasts of Norway, the Balearic Sea (NW Mediterranean), the Gulf of Genoa, the northern Aegean Sea, the eastern part of the Black Sea and the northern sea area of Cyprus that is located at the lee side of the Taurus Mountains

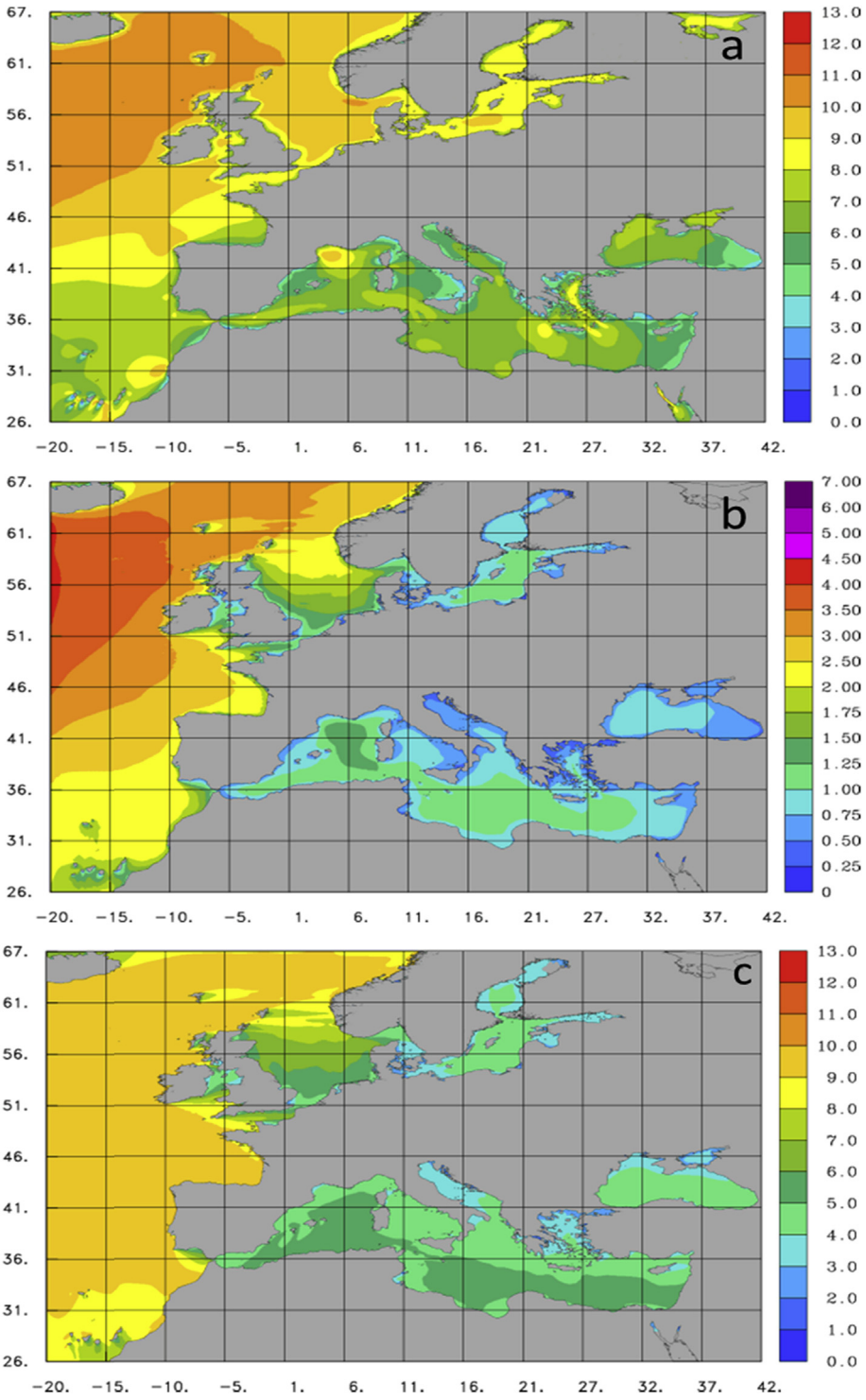

Fig. 7. Spatial distribution of the mean a) wind speed (m/s) at 80 m, b) significant wave height (m) and c) energy period (s), for the period 2001–2010.

(Fig. 9).

The variability of the available power resource in an interannual scale was estimated using, the ratio of the yearly mean values divided by the 10-year average (interannual variability index). According to this analysis the available wind and wave power potential revealed a profound spatiotemporal variability as illustrated in Figs. 10 and 11. This can be linked to large scale atmospheric features such as the NAO. The position and intensity of such large scale motions over the years can directly affect the spatial distribution of the power resource. It is also evident, that in an interannual scale the variation of wave power follows that of wind (Figs. 10 and 11).

The wind and wave power potential exhibits a profound seasonal variability as it can be seen in Figs. 12 and 13. The highest values for both resources are met during the winter months (December–February) (Figs. 12a and 13a). In particular, the NW coasts of Europe that are exposed to the Atlantic Ocean, are the most energetic areas during this season. This is the result of the intense mid-latitude cyclonic activity during this period and the positive NAO. Secondary power maxima are observed off the western coasts of the Iberian Peninsula, the Bay of Biscay and off the western coasts of Norway. During the cold season, the Mediterranean Sea is also characterized by intense cyclogenetic activity that is reflected to the wind and wave field, resulting to elevated wind and wave power resources (Figs. 12a and 13a). The same behavior, with rather reduced overall potential, is evident during the transient seasons from March–May and from September–November. This is evident in Figs. 12b and d, 13b and d.

During the summer months, June to August, the wind and wave power resource is rather weak (Figs. 12c and 13c). However, the Atlantic facing coasts of Europe are still experiencing rather high wind and wave energy values. Despite the fact that the wave resource is rather uniform over the major basins, the wind potential exhibits several localized maxima. Such areas are located off the western coasts of the Iberian Peninsula, off the southern and southwestern coasts of Norway, in the Gulf of Lions and in the Baltic and Aegean Sea (Figs. 12c and 13c). The wind climate in these regions has the lowest seasonal variability. However, this is not the case for the wave climate.

Estimating the higher moments, skewness and kurtosis, we gain information about the shape of the PDF that describes the wind and wave power density and about the potential influence by extremes. The highest skewness and kurtosis values are estimated for areas located in closed basins. These increased values indicate that the data are non-symmetric, with small mean values and long heavy tails to the right. This can be characterized as an unstable behavior

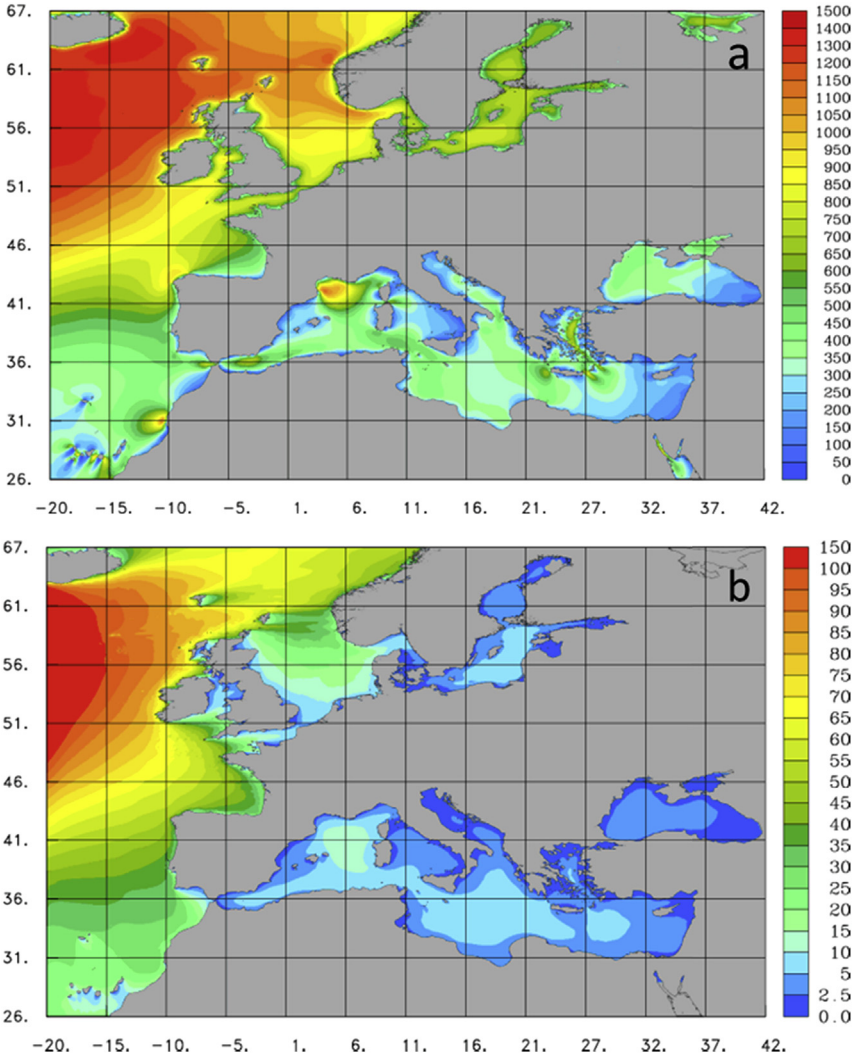

Fig. 8. Spatial distribution of a) mean wind power potential (W/m^2) at 80 m and b) wave power potential (kW/m), for the period 2001–2010.

and should be considered in the final decision. On the contrary, open seas seems to have a smoother behavior as the lower skewness and kurtosis values indicate (Fig. 14).

Regions of increased wind and wave power potential levels, low variability and small potential impact from extremes are primarily those exposed to the Atlantic Ocean. However areas with similar characteristics can also be found in enclosed sea areas. Such examples are the Gulf of Lions (NW Mediterranean), the Strait of Sicily (Central Mediterranean), the southwestern Baltic Sea and some localized sub-regions in the Aegean and the Ionian Seas (NE Mediterranean).

4.2. Correlation between wind and wave power resource

After identifying the long-term variability of the two resources, we assess the correlation between them in an hourly basis. It should be noted that their diversification is a key determinant for a combined exploitation. Taking advantage of their different characteristics, it is possible to result in a final output with reduced variability compared to the one produced from exploiting a single resource. Basically, we are seeking for sites where the correlation between wind and wave power potential is medium to low, indicating that the peaks in both resources do not occur at the same time. Moreover the offset in time of the maximum correlation gives the lag between the wind and wave field. Toward this direction the two resources were further analyzed in terms of correlation using the Pearson product-moment correlation coefficient.

$$c(\tau) = N^{-1} \sum_{i=1}^{N-\tau} \left[x_i - \mu_\chi\right] \left[y_{i+\tau} - \mu_y\right] \Big/ \sigma_\chi \sigma_y \tag{15}$$

where τ is the time-lag between wind (x_i) and wave power (y_i). The mean and standard deviation of wind and wave power are expressed by μ_χ, μ_y and σ_χ, σ_y respectively. $c(\tau) = 0$ means that there is no correspondence between the two resources while $c(\tau) = 1$ denotes a strong correlation.

For this analysis the most energetic areas were categorized according to nine possible wind and wave power combinations based on Table 3 and illustrated in Fig. 15. The thresholds for the wind power classes are based on the European Wind Atlas for Open Seas, produced by Riso National Laboratory [66] and the wave power thresholds on the ORECCA project [29]. In order to limit our study to deep offshore waters, the depth was selected to be more than 50 m and less than 500 m [29]. According to this classification, 21 sites near locations of interest were selected, as provided by the

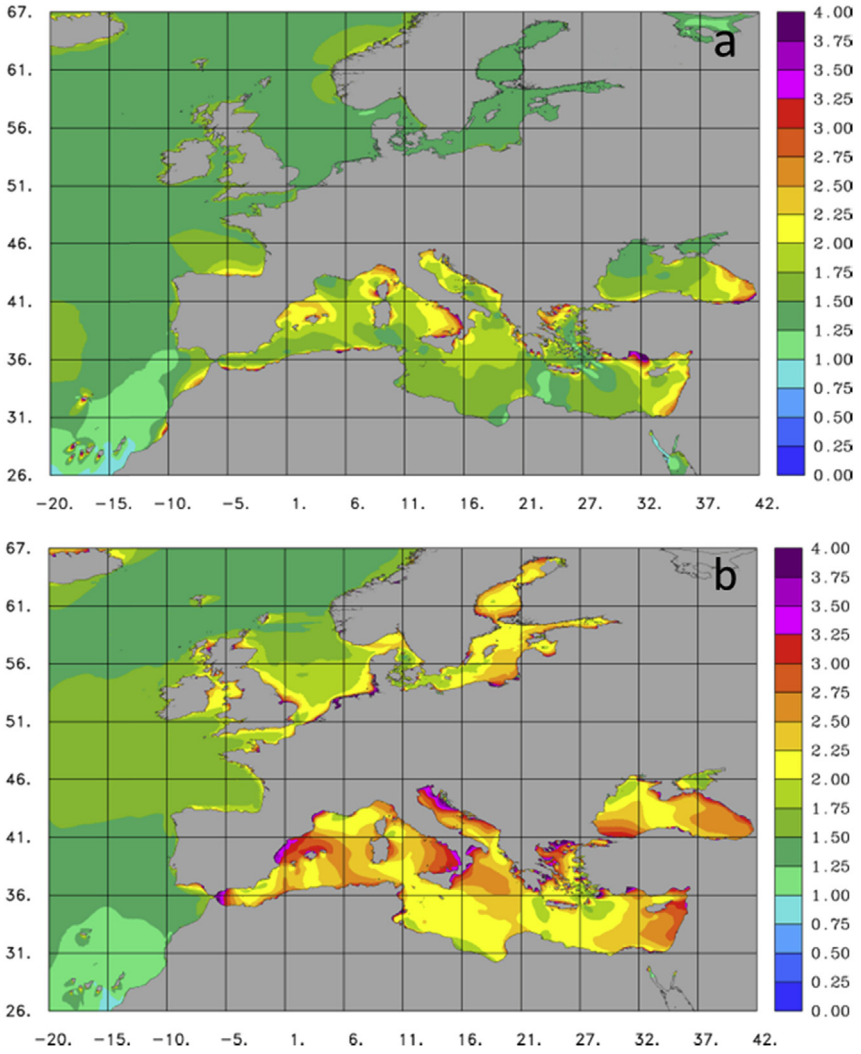

Fig. 9. Spatial distribution of the coefficient of variation, expressed as the standard deviation normalized to the mean value of the a) wind power potential at 80 m and of the b) wave power potential, for the period 2001–2010.

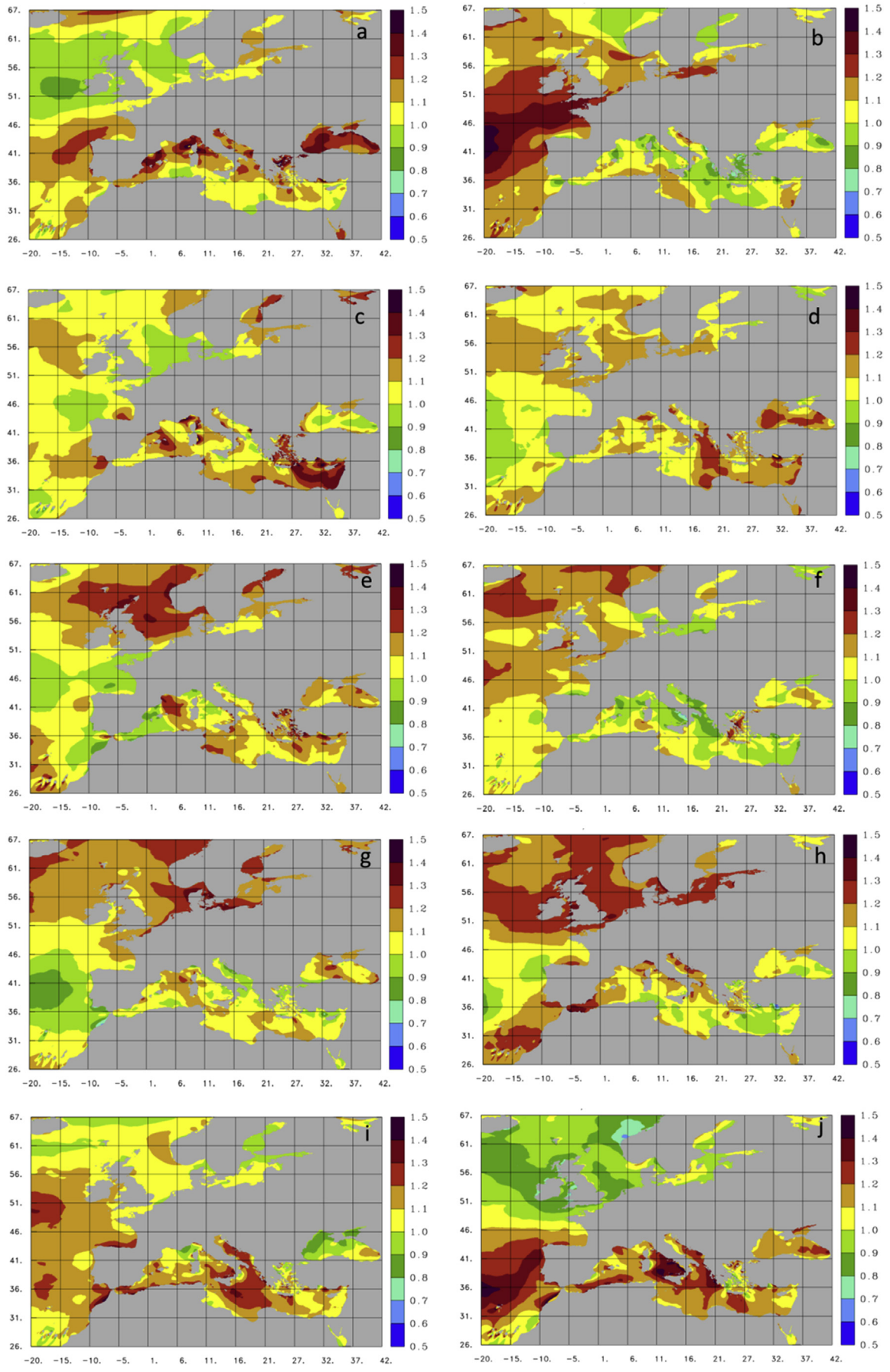

Fig. 10. Spatial distribution of the inter-annual variability index, defined as the mean yearly value divided by the mean 10-year value, of the wind power potential during the period 2001 to 2010 (a–j).

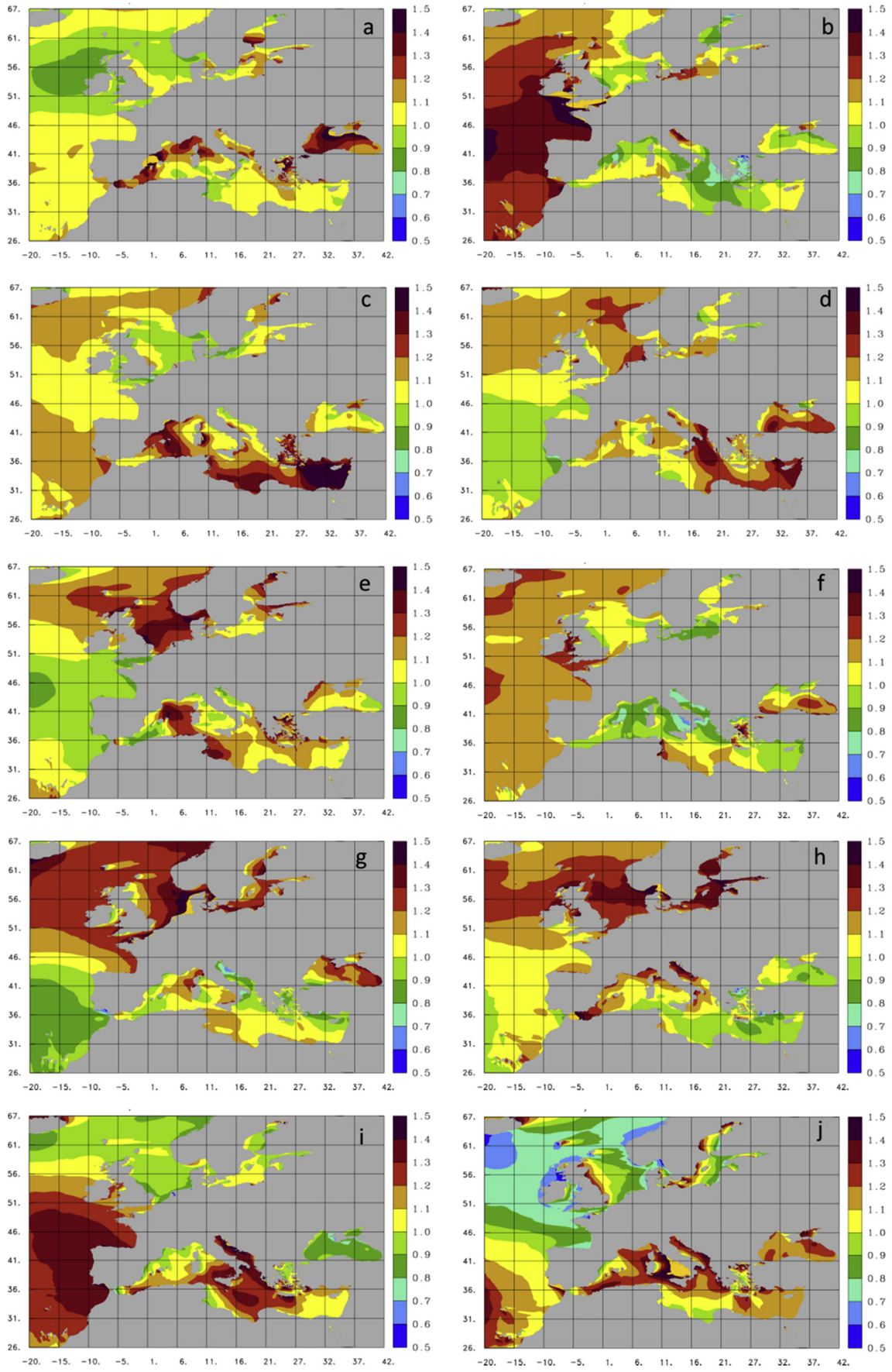

Fig. 11. Spatial distribution of the inter-annual variability index, defined as the mean yearly value divided by the mean 10-year value, of the wave power potential during the period 2001 to 2010 (a–j).

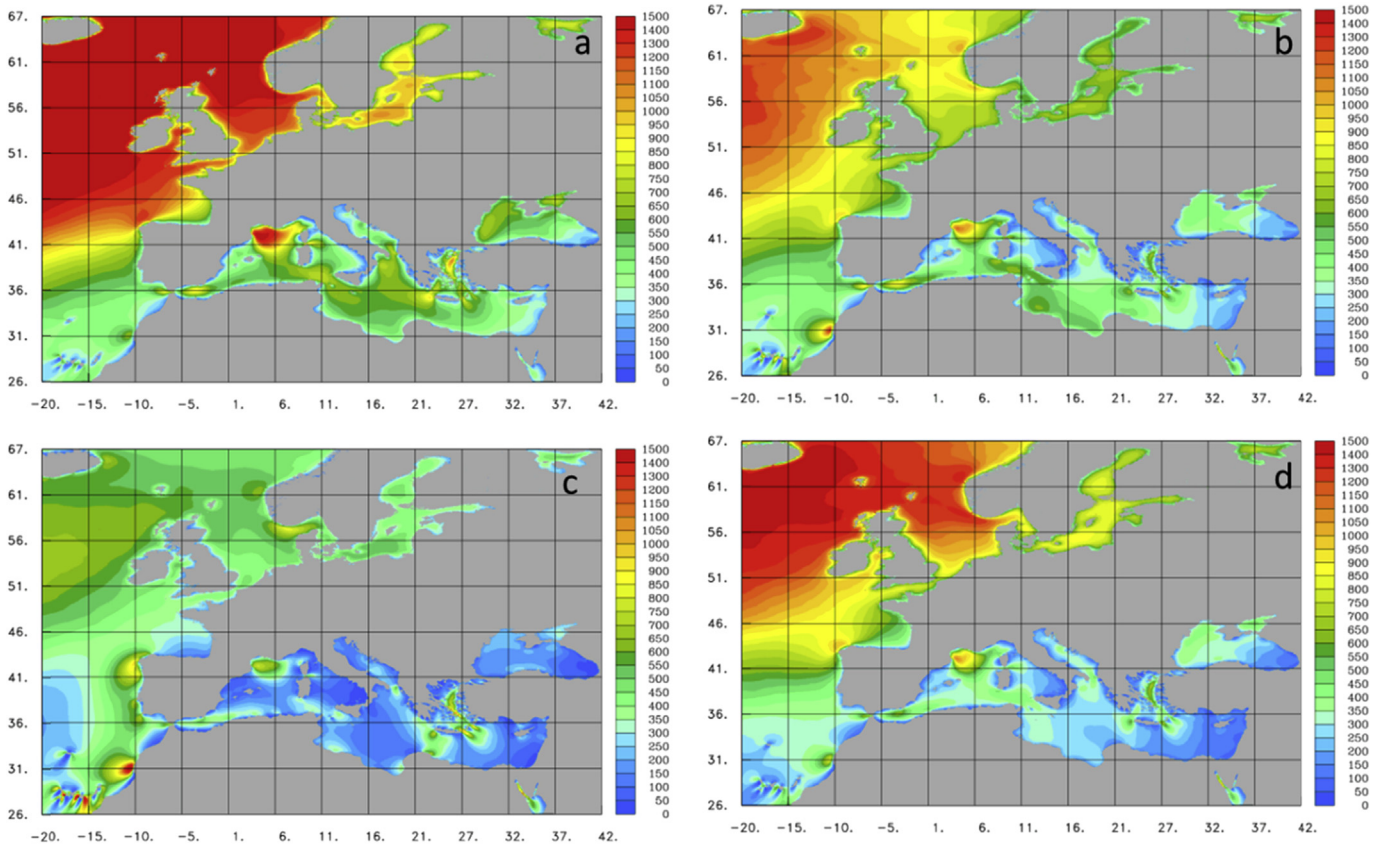

Fig. 12. Spatial distribution of the seasonal behavior of the mean wind power potential (W/m^2), for the period 2001–2010. The selected seasons are: a) December–January-February, b) March-April- May, c) June-July-August and d) September-October-November.

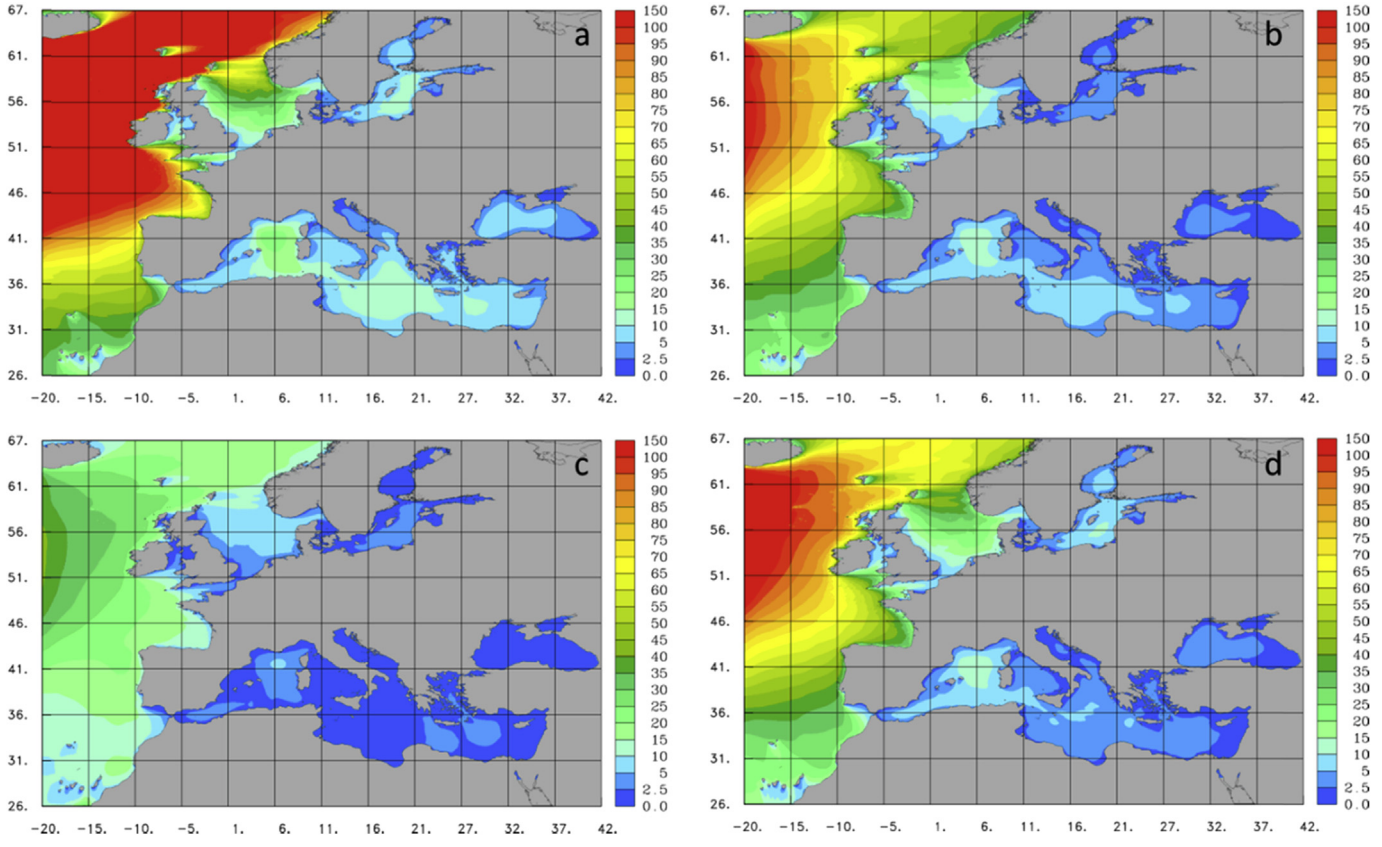

Fig. 13. Spatial distribution of the seasonal behavior of the mean wave power potential (kW/m), for the period 2001–2010. The selected seasons are: a) December–January-February, b) March-April- May, c) June-July-August and d) September-October-November.

MARINA platform project [30,31] and illustrated in Fig. 15. The selection was made in such way so as to cover the most important areas with considerable available resources. The correlation between the two resources was estimated for the 10-year period and for each season, separately.

The results of this analysis are presented in Table 4 and Tables 9–11 in Appendix 6.2. The areas that revealed the lowest correlation between wind and wave power are these exposed to the long Atlantic fetch. In particular, the areas located off the western coasts of the Iberian Peninsula and off the Canary Islands are the ones with the lowest values. At these areas the wave resource follows the wind resource with rather high time delay that varies within different timescales. As we move northward the correlation between wind and wave power increases.

In the wind driven sea areas like the Gulf of Lions, the Aegean and the Baltic Sea the two resources are strongly correlated. The positive strong correlation at zero lag indicates that the wave field is strongly controlled by the wind field as shown in Table 4 and Tables 9–11 in Appendix 6.2. This is mainly due to the limited extend of the basins that does not favor the creation of strong swells. This behavior is evident in the Mediterranean, in the English Channel and in the Baltic Sea. One indicative exception is the area west of Sassari, Sardinia. This is because, the area is exposed to the waves that initially generate in the Gulf of Lions and then propagate easterly. Sassari exhibits medium wind and low wave power (Table 4).

The seasonal and the inter-annual variability of the correlation between the two resources, is higher in the southwestern open sea areas of Europe as shown in Tables 9–11 in the Appendix 6.2. On the contrary, a more stable behavior within the seasons and the years characterizes the northwestern offshore areas of Europe and the wind driven ones. The sites that are located in sheltered areas with small fetches have the most stable behavior. Finally, there are sites located in the most energetic areas of Europe (e.g Belmullet, Lewis Isles and Faroe Isles, Stadvind, etc) where the two resources have satisfactory low correlation values (0.5–0.6) and a very stable behavior within the seasons.

For a more detailed analysis in different timescales the Villano Sisargas site was selected as representative and was further analyzed. At this site the highest amounts of wave power are from the NW while the highest amounts of wind power are from the NE or the SW (Fig. 16). In this open sea area the correspondence between wind and wave power is rather low (Table 4, Fig. 17). This is mainly due to the fact that the wave power resource is primary influenced by the Atlantic swell while the wind power resource is primary controlled by the local weather conditions. At this site the mean timelag within the 10-year period is 5 h with a maximum correlation of 0.4. However the maximum correlation and the corresponding timelag vary significantly during the months and during the years (Fig. 17).

The opposite is the case for the closed and semi-enclosed basins that are mainly wind driven areas. There, the correspondence is high and the time lags of a few hours (Table 4). As an indicative site to support our argument, a site located in the Baltic Sea was selected. In this sheltered area of limited fetch, the dominant southwesterly wind flow drives the southwesterly wave flow, as the overlapping directions show (Fig. 18). The high correlation, for the 10-year period, between the two resources at zero timelag (0.84) and the high maximum correlation at a 3-h timelag (0.89) point also to this direction (Table 4).

Based on the estimation of the correlation coefficient and the associated time lags in different timescales, it is evident that in wind driven areas (e.g Baltic Sea) the correlations are high and the lags low. This behavior seems to be stable during each month

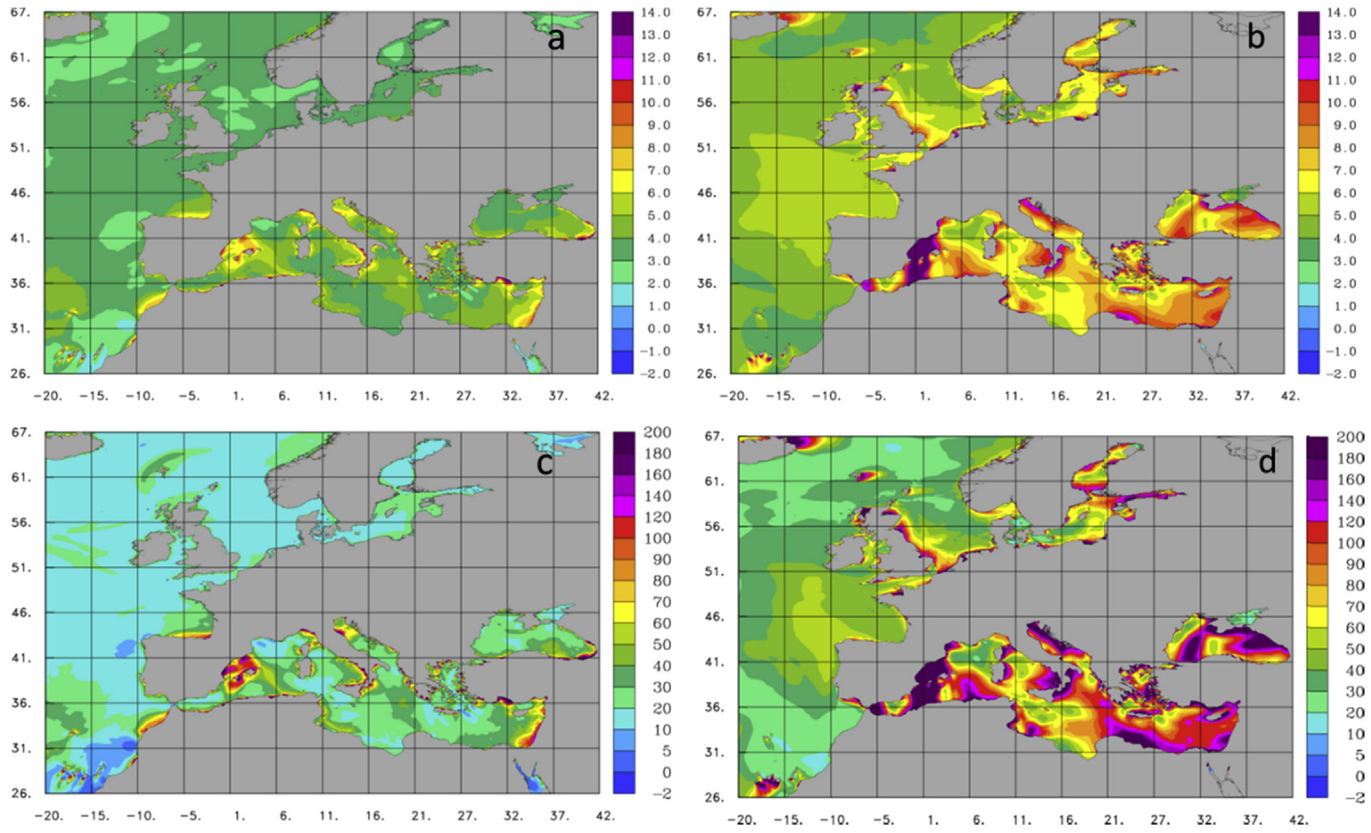

Fig. 14. a, b) Skewness and c, d) kurtosis of the wind power potential at 80 m and the wave power potential respectively, for the period 2001–2010.

Table 3
Selected categories for combined wind and wave power resource characterization.

Characterization	Wind power (W/m^2)	Wave power (kW/m)
Low	200–400	5–15
Medium	400–600	15–25
High	>600	>25

50 m < Bathymetry < 500 m

within the 10-year period as the small variability indicates (illustrated as error-bars in Fig 19). The opposite is the case for the open sea areas which are represented here by the Villano Sisargas site (Fig 17). Thus in order to extract more solid conclusions it is important to study the correspondence of the two resources in several time scales.

4.3. Combined exploitation of wind and wave power resource

Harvesting the available resource and turn it to power is a challenging procedure. Wind power industry has already converged to a standard type of wind turbine for power extraction, while wave power has not yet reached to that point. Several competing prototypes, based on different working principles, are currently tested in different areas. The main scope is to optimally fit them to the local environmental conditions.

One way to associate the theoretical power resource with the actual power output of the device is to use environmental matrices, provided either from observations or numerical models, along with the power curves/tables of the specific device used [25,67].

Following this approach, the benefits of the joint exploitation were analyzed using two hypothetical combined wind and wave energy conversion concepts. They are both based on typical energy converters, designed for deep offshore areas. The first Combined Concept (CC1) consists of a 5 MW Wind Turbine (WT) and a 7 MW Wavedragon Wave Energy Converter (WEC), resulting to an overall 12 MW rated power. The wind turbine used is a 5 MW fixed monopile. The power curve is presented in Fig. 21 (see Appendix 6.3). Wavedragon is a floating, slack moored overtopping device operating in water depths greater than 25 m [68]. The power matrix of the WEC is given in Table 12 (see Appendix 6.3). For the second Combined Concept (CC2), a 5 MW WT and ten 750 kW Pelamis WECs were selected, resulting to a system of an overall 12.5 MW rated power. Pelamis is a floating/submerged WEC that operates in water depths >50 m. The rated power and the power matrix are illustrated in Table 13 (see Appendix 6.3). The number of Pelamis used at the second concept (CC2) was such that CC1 and CC2 are comparable in terms of rated power. Their performance was compared against the individual devices (WT, Wavedragon and Pelamis) at two locations, with different metocean characteristics. The first one is Villano Sisargas that is located in a typical swell dominated area exposed to the Atlantic Ocean, while the second is located in a typical wind sea area offshore of Malta, in the Mediterranean.

The variability of the power output, within the 10-year period, is quantified in terms of standard deviation normalized by the mean value (CV) and in terms of percentage of zero production over the total number of hours considered. For Villano Sisargas the joint exploitation of the available wind and wave power resource, by both combined concepts, seems to reduce the overall variability of the final power output (Table 5). The opposite is the case for Malta (Table 6).

The most important outcome from the combined utilization of the available resource is the reduction of the hours with zero production. For Villano Sisargas that is an area where winds and waves reveal low correspondence (~0.36 see Table 4), the number of hours with zero output have been reduced nearly 10% compared to the individual devices, while the capacity factor is about 35% that is a satisfactory value (Table 5). In Malta, where the wind and wave conditions are strongly correlated (~0.77 see Table 4) the combined

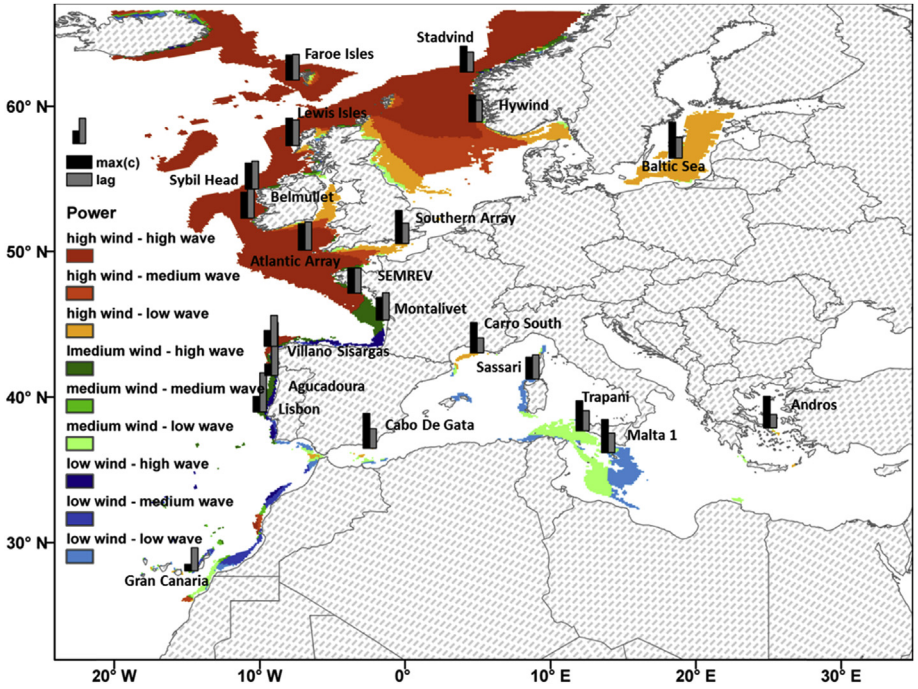

Fig. 15. Spatial distribution of the combined wind and wave power resource according to the nine clusters selected based on Table 3. The areas presented are deep offshore with depths ranging between 50 and 500 m. The twenty one sites, selected for correlation analysis between wind and wave resource are also illustrated. For each site the maximum correlation coefficient and the corresponding lag, for the 10-year period (2001–2010), are presented.

Table 4
The correlation between wind and wave power as expressed through the Pearson product moment correlation coefficient at zero time lag (c(0)) and through the maximum value of the coefficient (max(C)) with the corresponding lag are presented, for the decade 2001–2010.

Area	Station	Lat	Lon	Cross-correlation		
				c (0)	Lag	max(c)
Gran Canaria	Gran Canaria	28.05	−14.70	0.147	3	0.15
Portugal	Lisbon	39.00	−10	0.335	6	0.37
Portugal	Agucadoura	41.50	−9.20	0.245	5	0.27
NW Spain	Villano Sisargas	43.50	−9.25	0.365	5	0.4
Biscay Bay	Montalivet	45.30	−1.55	0.526	4	0.57
Biscay bay	SEMREV	47.15	−3.50	0.596	4	0.63
English Channel	Southern Array	50.55	−0.2	0.78	3	0.83
SW England	Atlantic Array	50.1	−6.9	0.62	4	0.66
W Ireland	Sybil Head	52.30	−10.85	0.596	5	0.65
W Ireland	Belmullet	54.30	−10.55	0.615	4	0.66
Scotland	Lewis Isles	57.30	−7.75	0.641	4	0.69
Scotland	Faroe Isles	61.80	−7.75	0.578	4	0.62
Norway	Hywind	58.95	4.85	0.62	3	0.66
Norway	Stadvind	62.35	4.25	0.61	3	0.66
Baltic Sea	Baltic Sea	56.45	18.6	0.84	3	0.89
SE Spain	Cabo de Gata	36.50	−2.45	0.831	3	0.87
Gulf of Lions	Carro South	43.05	4.95	0.71	2	0.73
Gulf of Lions	Sassari	41.25	8.75	0.495	3	0.54
Sicily strait	Malta 1	36.20	13.95	0.774	3	0.83
Sicily strait	Trapani	37.70	12.20	0.692	3	0.74
Aegean Sea	Andros	37.90	25.10	0.758	2	0.77

concepts didn't improve significantly the final output (Table 6). The hours of zero production using the combined concepts were only slightly reduced, ~1%, compared to that of the WT operating alone (Table 6). Finally, comparing the two hypothetical concepts, the one based on Pelamis seems to be more suitable than the one based on Wavedragon for both sites.

For Villano Sisargas, the final combined output is quite normally distributed as the low skewness and kurtosis values indicate (Table 5). For Malta, the higher values of skewness and kurtosis describe an aggregate power output that is more unstable. However, for the latter the most suitable concept seems to be the WT alone. The two combined concepts, CC1 and CC2, did not give the expected results in terms of variability reduction. This can be attributed to the specific climatological characteristics of the area and the fact that the two resources are strongly correlated.

Based on the aforementioned analysis, it is evident that is of great importance to accurately know the basic characteristics of the local wind and wave field. This information is important for the selection of the optimal WT and WEC combination that will result to a less variable power output, with less hours of zero production.

5. Conclusions

In this work a wind and wave energy resource assessment was performed for the offshore areas of Europe. The main objective was to identify the most important characteristics of the two resources in terms of availability, coherence, variability and correlation and their impact on the combined exploitation. In particular, the merits

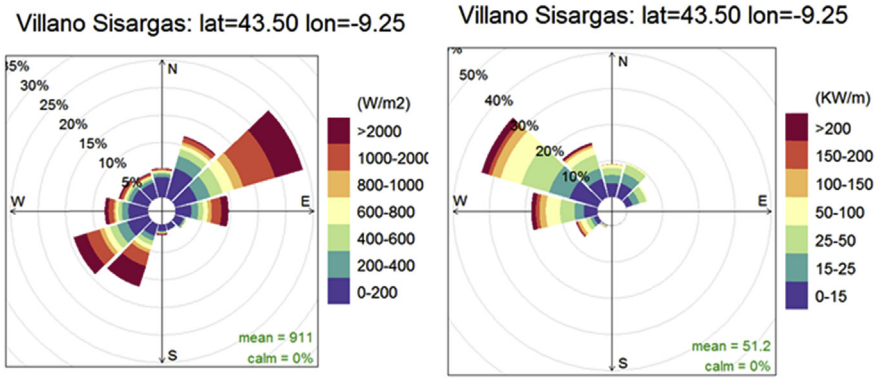

Fig. 16. Directional distribution of the wind power potential at 80 m (left) and wave power potential (right) in the NW tip of the Iberian Peninsula – Villano Sisargas, for the period 2001–2010.

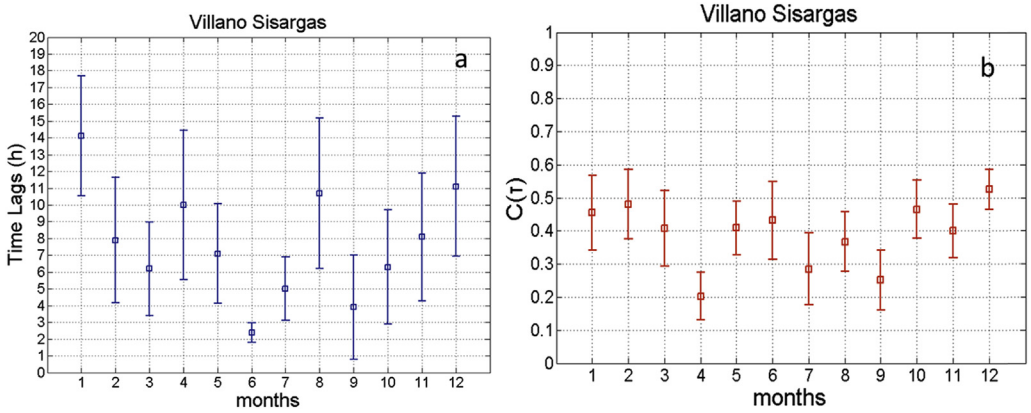

Fig. 17. a) Monthly time lags in hours between wind and wave power and the corresponding b) monthly maximum correlation coefficients along with the associated standard deviation within the years (illustrated as error-bars) for the NW tip of the Iberian Peninsula - Villano Sisargas, for the period 2001–2010.

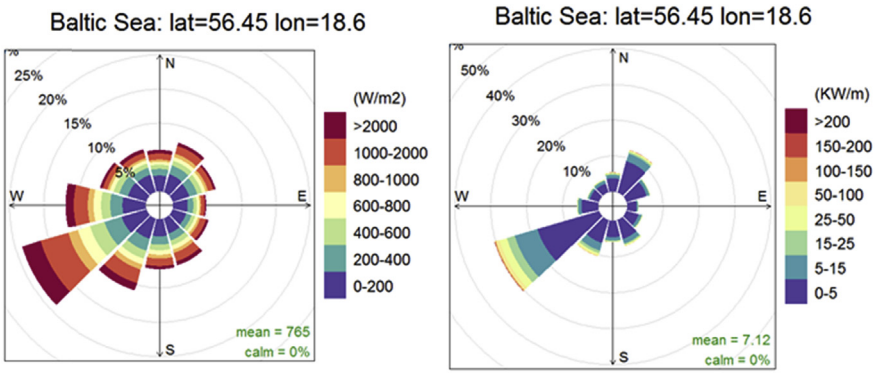

Fig. 18. Directional distribution of the wind power potential at 80 m (left) and wave power potential (right) in Baltic Sea, for the period 2001–2010.

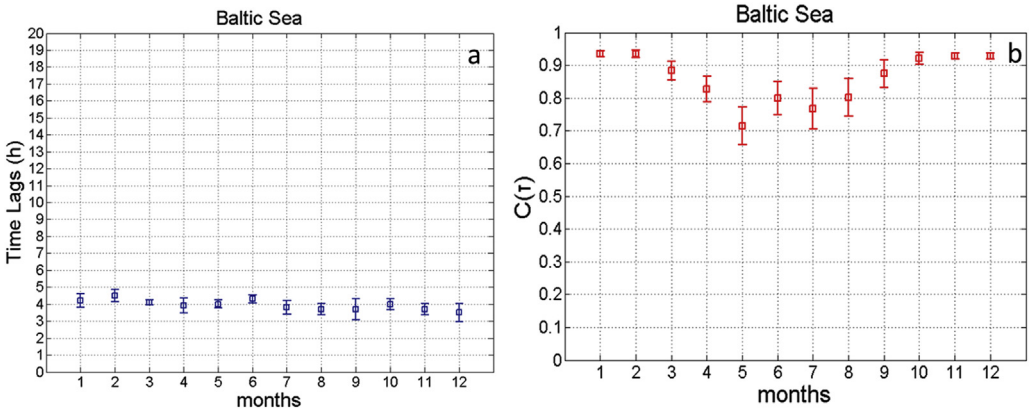

Fig. 19. a) Monthly time lags in hours between wind and wave power and the corresponding b) monthly maximum correlation coefficients along with the associated standard deviation within the years (illustrated as error-bars) in the Baltic Sea, for the period 2001–2010.

Table 5
Power statistics for Villano Sisargas site using the following single and combined converters: a 5 MW WT, a 7 MW Wavedragon WEC, ten Pelamis WECs (750 kW each) and the two combined concepts (CC1 and CC2). The analysis was performed for the period 2001–2010.

Villano sisargas	WT	Wavedragon	Pelamis	(CC1)	(CC2)
Power converters				WT + Wavedragon	WT + Pelamis
Rated Power (MW)	5.00	7.00	7.50	12.00	12.50
Mean (MW)	2.60	1.95	1.97	4.55	4.58
CV	0.78	0.85	0.72	0.66	0.67
Skewness	0.02	1.41	1.17	0.50	0.38
Kurtosis	1.32	4.53	4.36	2.45	1.99
Zero production (hrs)	8595	5304	3681	732	497
Zero production (%)	10	6	4	0.8	0.5
Capacity Factor (%)	52.07	27.84	26.29	34.94	36.60

Table 6
Power statistics for Malta 1 site using the following single and combined converters: a 5 MW WT, a 7 MW Wavedragon WEC, ten Pelamis WECs (750 kW each) and the two combined concepts (CC1 and CC2). The analysis was performed for the period 2001–2010.

Malta 1	WT	Wavedragon	Pelamis	(CC1)	(CC2)
Power converters				WT + Wavedragon	WT + Pelamis
Rated Power (MW)	5.00	7.00	7.50	12.00	12.50
Mean (MW)	1.58	0.41	0.54	1.99	2.12
CV	1.15	2.00	1.73	1.21	1.21
Skewness	0.90	3.99	2.63	1.28	1.25
Kurtosis	2.26	24.53	11.16	3.95	3.52
Zero production (hrs)	18003	52219	45715	16760	15404
Zero production (%)	20	59	52	19	17
Capacity Factor (%)	31.62	6.67	7.23	16.59	16.98

of a joint exploitation, using specific combined concepts in areas with different characteristics, were further analyzed. This study was performed using hindcast data from numerical simulations.

The resource assessment indicated that the areas with the highest wind and wave power density are the northwestern coasts of Europe. However moving southwards, the power resource is getting lower but it is still significant. The intensity and spatial distribution of the power potential over the area differs from season to season and from year to year. This variability is strongly linked to the intensity and position of the large scale atmospheric systems.

Contrary to it, the closed basins (due to their limited fetch) reveal rather weak wave energy potential and rather unstable conditions in terms of variability and impact from infrequent conditions. However there are several wind energy hotspots that are comparable to the most energetic locations of northwestern Europe.

When discussing about the combined use of the wind and wave power, the main aim is to deliver a less variable output to the energy grid. This can be achieved by understanding and efficiently handling the variability of the two resources. Areas ideal for combined use are these, where the two resources are less affected by extremes, have elevated mean values, stable behavior and finally low correlation. An extended time lag between the peaks of the wind and the wave energy field will result to a smoother final output with less hours of zero production. For Europe, areas with such characteristics are these exposed to the long Atlantic fetch. At these regions the wind and wave fields are the result of different weather conditions: The wave field is strongly controlled by the remote-generated Atlantic swell and the wind field by the local weather conditions. The lowest correlation between them is met in the southwestern coasts of Europe. For the enclosed sea areas the opposite is true.

The most important benefit of the joint exploitation of wind and wave energy resources is a less variable output with fewer hours of zero production, compared to that produced from an individual wind energy converter. The merits from the combined use are negligible in areas with wind-driven wave dominance. The opposite is true in the swell dominated ones. These are always areas with low correlation between wind and waves.

Finally it has to be pointed out that the theoretically-estimated wind and wave power density can only give a measure of the effective power. However, when it comes to actual devices the extracted power is determined, apart from the available potential, by the specific characteristics of the device. In this sense, for the optimal combined exploitation of the available wind and wave energy resource, the key issue is to successfully link the prevailing weather characteristics of the area with the main characteristics of the converters used.

Acknowledgments

The present work was supported by the European Commission through the 7th Framework Program (MARINA Platform – Marine Renewable Integrated Application Platform, Grant Agreement 241402). For the provision of the Italian buoy data we would like to thank the ISPRA's Rete Ondametrica Nazionale. For the FINO1 data provision we want to acknowledge the BMWi (Bundesministerium fuer Wirtschaft und Energie, Federal Ministry for Economic Affairs and Energy) and the PTJ (Projekttraeger Juelich, project executing organisation). For the provision of the Docking Shoal data we want to acknowledge the Crown Estate (Marine data exchange). Finally, we would like to thank the reviewers for their constructive comments.

6. Appendix

6.1. Buoy data

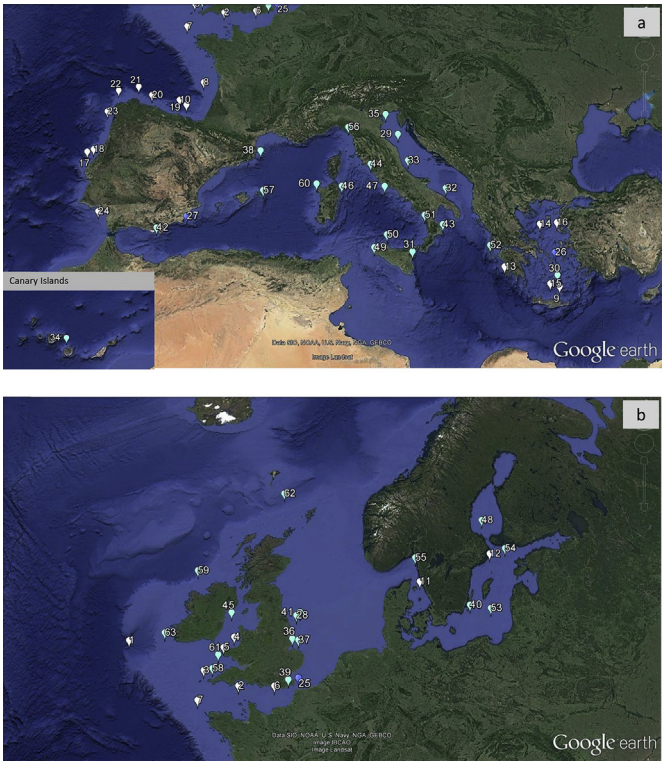

Fig. 20. Locations of the buoys used. The areas illustrated are: a) The Mediterranean and the SW offshore areas of Europe b) The North Sea, the Baltic Sea and the NW offshore areas of Europe. The labels correspond to the indexes in Tables 7 and 8 The color selected for each buoy indicates the availability: White markers: wind speed at 10m and Hs, Blue marker: Only wind speed at 10m, Light green: Only Hs data.

Table 7
Information regarding the location of the buoys, the available period and the number of data used in the evaluation analysis of the wind field. The indexes refer to the labels in Fig. 20.

Index	Lat	Lon	Duration	Entries	Index	Lat	Lon	Duration	Entries
1	50	−13,3	2010	604	**15**	35,8	24,9	2007–2010	6807
2	49,9	−2,9	2007–2010	30309	**16**	39,15	25,81	2004–2010	9730
3	50,1	−6,1	2007–2010	29894	**17**	39,5	−9,65	2010	1273
4	52,3	−4,5	2009–2010	8405	**18**	39,75	−9,2	2010	2222
5	51,6	−5,1	2009–2010	9709	**19**	43,65	−3,05	2002–2010	51362
6	50,4	0	2007–2010	28000	**20**	43,75	−6,2	2002–2010	61398
7	48,5	−5,8	2001–2010	51776	**21**	44,05	−7,65	2002–2010	50557
8	45,2	−2,3	2001–2010	73063	**22**	43,5	−9,25	2002–2010	51952
9	35,6	25,6	2004–2006	5917	**23**	42,1	−9,4	2002–2010	60507
10	43,85	−3,75	2007–2010	20435	**24**	36,5	−7	2002–2010	64367
11	57,2	11,55	2001–2008	34383	**25**	51,1	1,8	2006–2010	31421
12	58,95	19,15	2001–2010	36117	**26**	37,5	25,45	2004–2010	12836
13	36,8	21,6	2007–2010	8131	**27**	37,55	−0,45	2007–2009	28135
14	39,1	24,45	2007–2010	6567					

Table 8
Information regarding the location of the buoys, the available period and the number of data used in the evaluation analysis of the wave field. The indexes refer to the labels in Fig. 20.

Index	Lat	Lon	Years	Entries	Index	Lat	Lon	Years	Entries
1	50	−13,3	2009–2010	9567	**34**	28,2	−15,8	2001–2004	30084
2	49,9	−2,9	2009–2010	5051	**35**	44,95	12,65	2002–2004	12125
3	50,1	−6,1	2009–2010	6973	**36**	53,05	0,5	2010	6582
4	52,3	−4,5	2009–2010	5164	**37**	53,05	1,05	2002–2003	10454
5	51,6	−5,1	2009–2010	6257	**38**	41,9	3,65	2001–2004	17206
6	50,4	0	2009–2010	2530	**39**	50,9	1	2008–2010	23379
7	48,5	−5,8	2010	814	**40**	56,07	16,68	2001–2010	18832
8	45,2	−2,3	2009–2010	8744	**41**	54,5	0,6	2010	5406
9	35,6	25,6	2004–2006	5918	**42**	36,55	−2,35	2001–2004	23489
10	43,85	13,7	2002–2004	15484	**43**	39	17,2	2002–2004	21576
11	57,2	11,55	2001–2009	33060	**44**	42	11,8	2002–2004	17123
12	58,95	19,15	2001–2010	37736	**45**	53,5	−5,45	2008–2010	4544
13	36,8	21,6	2007–2010	8222	**46**	40,6	9,9	2002–2004	16190
14	39,1	24,45	2007–2010	6887	**47**	40,85	12,95	2001–2008	36464
15	35,8	24,9	2007–2009	7432	**48**	60,9	18,6	2006–2010	33610
16	39,15	25,81	2006–2010	11851	**49**	37,5	12,55	2002–2004	18880
17	39,5	−9,65	2009–2010	5215	**50**	38,25	13,35	2002–2004	19650
18	39,75	−9,2	2010	2049	**51**	39,45	15,9	2002–2004	20810
19	43,65	−3,05	2002–2010	48565	**52**	37,95	20,6	2007–2010	6662
20	43,75	−6,2	2002–2010	54901	**53**	55,9	18,8	2005–2010	31431
21	44,05	−7,65	2002–2010	53031	**54**	59,25	21	2005–2010	30198
22	43,5	−9,25	2002–2010	58086	**55**	58,5	10,95	2005–2010	47116
23	42,1	−9,4	2002–2010	61674	**56**	43,95	9,85	2002–2004	13907
24	36,5	−7	2002–2010	35384	**57**	39,75	4,45	2001–2004	6546
28	54,3	0,35	2003–2004	5548	**58**	50,35	−5,45	2005–2007	3246
29	43,85	−3,75	2007–2010	20611	**59**	55	−10	2008–2010	11861
30	36,25	25,5	2004–2010	13658	**60**	40,55	8,1	2002–2004	15818
31	37,45	15,15	2002–2004	21039	**61**	51,15	−5,35	2004–2005	6881
32	41	17,4	2002–2004	17590	**62**	60,7	−4,5	2009–2010	7374
33	42,4	14,55	2002–2004	13566	**63**	51,2	−10,55	2008–2010	15636

6.2. Cross-correlation statistics: Seasonal analysis

Table 9
The seasonal analysis of cross-correlation c(0) between wind and wave power, at zero time lag, for 21 sites is presented. For each season the mean and standard deviation of the c(0) are presented. An overall mean value is estimated for all seasons (presented in column 6) and a seasonal variability index (S%) is calculated from the standard deviation of the mean seasonal values divided by their mean value (column 7).

Cross-correlation at zero lag C (0)						
	DJF	MAM	JJA	SON	Mean	S (%)
Gran Canaria	0.33 ± 0.17	0.26 ± 0.11	0.55 ± 0.11	0.13 ± 0.12	0.32	55.36
Lisbon	0.31 ± 0.14	0.32 ± 0.15	0.50 ± 0.16	0.42 ± 0.12	0.39	23.21
Agucadoura	0.34 ± 0.11	0.23 ± 0.14	0.35 ± 0.18	0.37 ± 0.12	0.32	19.51
Villano Sisargas	0.41 ± 0.13	0.33 ± 0.14	0.30 ± 0.16	0.34 ± 0.13	0.35	13.49
Montalivet	0.53 ± 0.08	0.45 ± 0.21	0.21 ± 0.22	0.35 ± 0.15	0.39	35.83
SEMREV	0.59 ± 0.06	0.51 ± 0.18	0.35 ± 0.2	0.46 ± 0.12	0.48	21.04
Southern Array	0.76 ± 0.06	0.76 ± 0.08	0.7 ± 0.1	0.79 ± 0.05	0.75	5.02
Atlantic Array	0.56 ± 0.1	0.55 ± 0.13	0.47 ± 0.1	0.59 ± 0.1	0.54	9.44
Sybil Head	0.52 ± 0.10	0.6 ± 0.11	0.47 ± 0.1	0.57 ± 0.06	0.54	10.58
Belmullet	0.54 ± 0 .0.1	0.6 ± 0.15	0.55 ± 0.11	0.57 ± 0.08	0.57	4.68
Lewis Isles	0.57 ± 0.09	0.61 ± 0.11	0.61 ± 0.07	0.60 ± 0.1	0.60	3.17
Faroe Isles	0.52 ± 0.08	0.54 ± 0.11	0.54 ± 0.18	0.54 ± 0.1	0.54	1.87
Hywind	0.62 ± 0.07	0.59 ± 0.12	0.68 ± 0.15	0.63 ± 0.1	0.63	5.94
Stadvind	0.59 ± 0.13	0.61 ± 0.1	0.57 ± 0.14	0.59 ± 0.08	0.59	2.77
Baltic Sea	0.86 ± 0.02	0.75 ± 0.06	0.72 ± 0.09	0.86 ± 0.03	0.80	9.18
Cabo de Gata	0.86 ± 0.05	0.81 ± 0.06	0.8 ± 0.04	0.81 ± 0.09	0.82	3.30
Carro South	0.73 ± 0.1	0.76 ± 0.09	0.84 ± 0.04	0.75 ± 0.12	0.77	6.27
Sassari	0.59 ± 0.08	0.36 ± 0.11	0.43 ± 0.10	0.50 ± 0.16	0.47	20.92
Malta 1	0.78 ± 0.04	0.76 ± 0.05	0.84 ± 0.06	0.78 ± 0.06	0.79	4.38
Trapani	0.72 ± 0.07	0.67 ± 0.06	0.6 ± 0.11	0.71 ± 0.12	0.68	8.07
Andros	0.86 ± 0.05	0.84 ± 0.05	0.88 ± 0.04	0.88 ± 0.05	0.87	2.21

Table 10
The seasonal analysis of the time lags between wind and wave power, for 21 sites is presented. For each season the mean and standard deviation of the time lags, are presented. An overall mean time lag is estimated for all seasons (presented in column 6) and a seasonal variability index (S%) is calculated from the standard deviation of the mean seasonal values divided by their mean value (column 7).

Time lags at max cross-correlation						
	DJF	MAM	JJA	SON	Mean	S (%)
Gran Canaria	6.7 ± 5.8	7 ± 6.6	5.4 ± 5.6	7 ± 6.3	6.53	11.70
Lisbon	14.7 ± 6.3	9.3 ± 5.1	4.9 ± 2.4	10 ± 7.5	9.73	41.25
Agucadoura	13.4 ± 7.7	11.5 ± 7	2.1 ± 1.10	7.4 ± 6.5	8.60	58.19
Villano Sisargas	7.9 ± 4.9	8.9 ± 6.75	4.9 ± 5.8	7.8 ± 6.8	7.38	23.36
Montalivet	5.5 ± 1.26	5.9 ± 2.8	3.9 ± 1.1	7.5 ± 7.45	5.70	25.94
SEMREV	4.9 ± 1.44	4.8 ± 2.4	4.4 ± 1.64	9.2 ± 6.3	5.83	38.80
Southern Array	4 ± 0.47	3.7 ± 0.48	3.6 ± 0.5	3.6 ± 0.6	3.73	5.08
Atlantic Array	6.2 ± 4.2	7.3 ± 5.01	6.3 ± 1.15	5.4 ± 2.06	6.30	12.36
Sybil Head	7.7 ± 4.9	5.4 ± 1.5	7.8 ± 5.4	5.9 ± 1.66	6.70	18.36
Belmullet	5.9 ± 0.87	6.1 ± 4.67	8.2 ± 6.5	5.5 ± 1.4	6.43	18.82
Lewis Isles	5.2 ± 0.9	4.9 ± 1.19	5.1 ± 1.3	4.9 ± 0.73	5.03	2.99
Faroe Isles	5.5 ± 0.97	5.1 ± 1.45	5.9 ± 2.9	5.5 ± 1.2	5.50	5.94
Hywind	4.3 ± 0.48	3.9 ± 0.56	3.5 ± 0.5	4.2 ± 0.78	3.98	9.04
Stadvind	4.4 ± 1.17	3.9 ± 0.6	6 ± 5.3	4.1 ± 0.56	4.60	20.78
Baltic Sea	4.2 ± 0.42	4.1 ± 0.3	4.1 ± 0.56	3.9 ± 0.56	4.08	3.09
Cabo de Gata	4 ± 0.47	4.1 ± 0.56	3.8 ± 0.63	3.7 ± 0.94	3.90	4.68
Carro South	2.8 ± 0.42	2.9 ± 0.56	3.2 ± 0.41	3 ± 0	2.98	5.74
Sassari	4.8 ± 1.03	4.3 ± 1.05	5.9 ± 1.10	4.9 ± 1.3	4.98	13.47
Malta 1	3.9 ± 0.3	4 ± 0.81	3.4 ± 0.5	4.4 ± 0.96	3.93	10.48
Trapani	4.1 ± 0.87	4 ± 0.47	4.1 ± 0.56	3.8 ± 1.03	4.00	3.54
Andros	2.3 ± 0.67	2.8 ± 0.63	3 ± 0.66	3.5 ± 0.7	2,90	17,13

Table 11
The seasonal analysis of the max cross-correlation between wind and wave power, for 21 sites is presented. For each season the mean and standard deviation of the time lags, are presented. An overall mean time lag is estimated for all seasons (presented in column 6) and a seasonal variability index (S%) is calculated from the standard deviation of the mean seasonal values divided by their mean value (column 7).

Max cross-correlation: max (C(τ))						
	DJF	MAM	JJA	SON	Mean	S (%)
Gran Canaria	0.36 ± 0.19	0.28 ± 0.11	0.57 ± 0.1	0.14 ± 0.12	0.34	53.24
Lisbon	0.40 ± 0.12	0.38 ± 0.14	0.51 ± 0.16	0.48 ± 0.13	0.44	14.10
Agucadoura	0.43 ± 0.07	0.28 ± 0.14	0.36 ± 0.18	0.42 ± 0.13	0.37	18.52
Villano Sisargas	0.46 ± 0.12	0.37 ± 0.15	0.32 ± 0.14	0.39 ± 0.14	0.39	15.07
Montalivet	0.59 ± 0.06	0.49 ± 0.24	0.28 ± 0.22	0.4 ± 0.19	0.44	29.98
SEMREV	0.63 ± 0.05	0.56 ± 0.2	0.39 ± 0.2	0.53 ± 0.11	0.53	19.11
Southern Array	0.81 ± 0.06	0.81 ± 0.06	0.75 ± 0.09	0.84 ± 0.05	0.80	4.70
Atlantic Array	0.61 ± 0.10	0.61 ± 0.12	0.54 ± 0.1	0.65 ± 0.09	0.60	7.59
Sybil Head	0.59 ± 0.10	0.65 ± 0.11	0.55 ± 0.06	0.63 ± 0.07	0.61	7.33
Belmullet	0.60 ± 0.10	0.64 ± 0.15	0.62 ± 0.08	0.64 ± 0.07	0.63	3.06
Lewis Isles	0.63 ± 0.09	0.66 ± 0.11	0.67 ± 0.07	0.66 ± 0.11	0.66	2.64
Faroe Isles	0.58 ± 0.08	0.59 ± 0.11	0.61 ± 0.18	0.6 ± 0.09	0.60	2.17
Hywind	0.67 ± 0.07	0.63 ± 0.12	0.71 ± 0.15	0.69 ± 0.08	0.68	5.06
Stadvind	0.65 ± 0.12	0.65 ± 0.1	0.63 ± 0.15	0.65 ± 0.08	0.65	1.55
Baltic Sea	0.92 ± 0.01	0.80 ± 0.05	0.78 ± 0.09	0.91 ± 0.01	0.85	8.53
Cabo de Gata	0.90 ± 0.04	0.86 ± 0.03	0.84 ± 0.04	0.85 ± 0.08	0.86	3.05
Carro South	0.75 ± 0.11	0.78 ± 0.09	0.88 ± 0.03	0.78 ± 0.11	0.80	7.12
Sassari	0.66 ± 0.09	0.39 ± 0.11	0.49 ± 0.10	0.55 ± 0.15	0.52	21.62
Malta 1	0.83 ± 0.03	0.82 ± 0.02	0.88 ± 0.05	0.84 ± 0.06	0.84	3.12
Trapani	0.78 ± 0.06	0.72 ± 0.06	0.66 ± 0.13	0.76 ± 0.11	0.73	7.25
Andros	0.87 ± 0.04	0.85 ± 0.04	0.89 ± 0.03	0.85 ± 0.04	0,87	2,21

6.3. Power Production Curve and Power Production Matrices for the converters used.

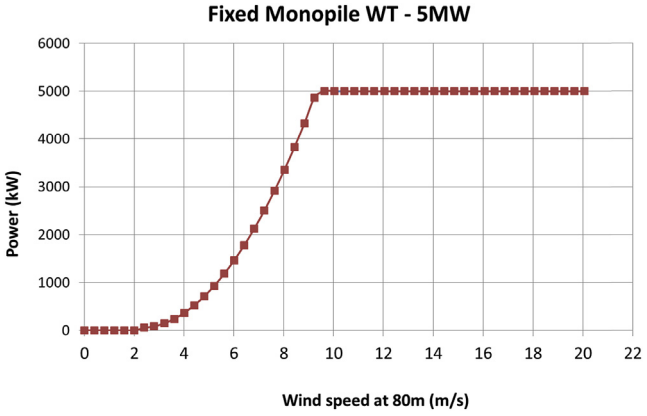

Fig. 21. Power curve of the 5 MW fixed monopile wind turbine.

Table 12
Wavedragon power matrix (in kW).

Hs(m) / Te(s)	5.0	6.0	7.0	8.0	9.0	10.0	11.0	12.0	13.0	14.0	15.0	16.0	17.0
1.0	160	250	360	360	360	360	360	360	320	280	250	220	180
2.0	640	700	840	900	1190	1190	1190	1190	1070	950	830	710	590
3.0	-	1450	1610	1750	2000	2620	2620	2620	2360	2100	1840	1570	1310
4.0	-	-	2840	3220	3710	4200	5320	5320	4430	3930	3440	2950	2460
5.0	-	-	-	4610	5320	6020	7000	7000	6790	6090	5250	3950	3300
6.0	-	-	-	-	6720	7000	7000	7000	7000	7000	6860	5110	4200
7.0	-	-	-	-	-	7000	7000	7000	7000	7000	7000	6650	5740

Table 13
Pelamis power matrix (in kW).

Hs(m) / Te(s)	5.0	5.5	6.0	6.5	7.0	7.5	8.0	8.5	9.0	9.5	10.0	10.5	11.0	11.5	12.0	12.5	13.0
0.5	-	-	-	-	-	-	-	-	-	-	-	-	-	-	-	-	-
1.0	-	22	29	34	37	38	38	37	35	32	29	26	23	21	-	-	-
1.5	32	50	65	76	83	86	86	83	78	72	65	59	53	21	42	37	33
2.0	57	88	115	136	148	153	152	147	138	127	116	104	93	47	74	66	59
2.5	89	138	180	212	231	238	238	230	216	199	181	163	146	83	116	103	92
3.0	129	198	260	305	332	340	332	315	292	266	240	219	210	130	167	149	132
3.5	-	270	354	415	438	440	424	404	377	362	326	292	260	188	215	202	180
4.0	-	-	462	502	540	546	530	499	475	429	384	366	339	230	267	237	213
4.5	-	-	544	635	642	648	628	590	562	528	473	432	382	301	338	300	266
5.0	-	-	-	739	726	731	707	687	670	607	557	521	472	356	369	348	328
5.5	-	-	-	750	750	750	750	750	667	667	658	586	530	417	446	395	355
6.0	-	-	-	-	750	750	750	750	750	750	711	633	619	496	512	470	415
6.5	-	-	-	-	750	750	750	750	750	750	750	743	658	558	579	512	481
7.0	-	-	-	-	-	750	750	750	750	750	750	750	750	621	613	584	525
7.5	-	-	-	-	-	-	750	750	750	750	750	750	750	676	686	622	593
8.0	-	-	-	-	-	-	-	750	750	750	750	750	750	750	750	690	625

References

[1] S. Astariz, C. Perez-collazo, J. Abanades, G. Iglesias, Co-located wave-wind farms : Economic assessment as a function of layout, Renew. Energy 83 (2015) 837–849, http://dx.doi.org/10.1016/j.renene.2015.05.028.

[2] L. Cradden, C. Kalogeri, I.M. Barrios, G. Galanis, D. Ingram, G. Kallos, Multi-criteria site selection for offshore renewable energy platforms, Renew. Energy 87 (2016) 791–806.

[3] S. Astariz, G. Iglesias, Enhancing wave energy competitiveness through co-located wind and wave energy farms, A Rev. Shad. Eff. Energies (2015) 7344–7366, http://dx.doi.org/10.3390/en8077344.

[4] S.B. Capps, C.S. Zender, Global ocean wind power sensitivity to surface layer stability, Geophys. Res. Lett. 36 (2009) 1–5, http://dx.doi.org/10.1029/2008GL037063.

[5] R.A. Arinaga, K.F. Cheung, Atlas of global wave energy from 10 years of reanalysis and hindcast data, Renew. Energy 39 (2012) 49–64, http://dx.doi.org/10.1016/j.renene.2011.06.039.

[6] Q. Jiang, J.D. Doyle, T. Haack, M.J. Dvorak, C.L. Archer, M.Z. Jacobson, Exploring wind energy potential off the California coast, Geophys. Res. Lett. 35 (2008) 1–6, http://dx.doi.org/10.1029/2008GL034674.

[7] G. Iglesias, M. Lopez, R. Carballo, A. Castro, J.A. Fraguela, P. Frigaard, Wave energy potential in Galicia (NW Spain), Renew. Energy 34 (2009) 2323–2333, http://dx.doi.org/10.1016/j.renene.2009.03.030.

[8] D. Vicinanza, P. Contestabile, V. Ferrante, Wave energy potential in the north-west of Sardinia (Italy), Renew. Energy 50 (2013) 506–521, http://dx.doi.org/10.1016/j.renene.2012.07.015.

[9] I. Karagali, M. Badger, A.N. Hahmann, A. Pena, C.B. Hasager, A.M. Sempreviva, Spatial and temporal variability of winds in the northern European seas, Renew. Energy 57 (2013) 200–210, http://dx.doi.org/10.1016/j.renene.2013.01.017.

[10] P. Lenee-Bluhm, R. Paasch, H.T. Ozkan-Haller, Characterizing the wave energy resource of the US Pacific Northwest, Renew. Energy 36 (2011) 2106–2119, http://dx.doi.org/10.1016/j.renene.2011.01.016.

[11] Z. Defne, K.A. Haas, H.M. Fritz, Wave power potential along the Atlantic coast of the southeastern USA, Renew. Energy 34 (2009) 2197–2205, http://dx.doi.org/10.1016/j.renene.2009.02.019.

[12] E. Rusu, C.G. Soares, Wave energy pattern around the Madeira Islands, Energy 45 (2012) 771–785, http://dx.doi.org/10.1016/j.energy.2012.07.013.

[13] J.E. Stopa, K.F. Cheung, Y.L. Chen, Assessment of wave energy resources in Hawaii, Renew. Energy 36 (2011) 554–567, http://dx.doi.org/10.1016/j.renene.2010.07.014.

[14] S.P. Neill, M.R. Hashemi, Wave power variability over the northwest European shelf seas, Appl. Energy 106 (2013) 31–46, http://dx.doi.org/10.1016/j.apenergy.2013.01.026.

[15] G. Zodiatis, G. Galanis, A. Nikolaidis, C. Kalogeri, D. Hayes, G.C. Georgiou, P.C. Chu, G. Kallos, Wave energy potential in the eastern Mediterranean levantine basin. An integrated 10-year study, Renew. Energy 69 (2014) 311–323.

[16] D.P. Dee, S.M. Uppala, A.J. Simmons, P. Berrisford, P. Poli, S. Kobayashi, U. Andrae, M.A. Balmaseda, G. Balsamo, P. Bauer, P. Bechtold, A.C.M. Beljaars, L. van de Berg, J. Bidlot, N. Bormann, C. Delsol, R. Dragani, M. Fuentes, A.J. Geer, L. Haimberger, S.B. Healy, H. Hersbach, E.V. Holm, L. Isaksen, P. Kallberg, M. Kohler, M. Matricardi, A.P. McNally, B.M. Monge-Sanz, J.J. Morcrette, B.K. Park, C. Peubey, P. de Rosnay, C. Tavolato, J.N. Thepaut, F. Vitart, The ERA-Interim reanalysis: configuration and performance of the data assimilation system, Q. J. R. Meteorol. Soc. 137 (2011) 553–597, http://dx.doi.org/10.1002/qj.828.

[17] S.M. Uppala, P.W. Killberg, A.J. Simmons, U. Andrae, V.D.C. Bechtold, M. Fiorino, J.K. Gibson, J. Haseler, A. Hernandez, G.A. Kelly, X. Li, K. Onogi, S. Saarinen, N. Sokka, R.P. Allan, E. Andersson, K. Arpe, M.A. Balmaseda, A.C.M. Beljaars, L. Van De Berg, J. Bidlot, N. Bormann, S. Caires, F. Chevallier, A. Dethof, M. Dragosavac, M. Fisher, M. Fuentes, S. Hagemann, E. Hólm, B.J. Hoskins, L. Isaksen, P.A.E.M. Janssen, R. Jenne, A.P. Mcnally, J.-F. Mahfouf, J.-J. Morcrette, N.A. Rayner, R.W. Saunders, P. Simon, A. Sterl, K.E. Trenberth, A. Untch, D. Vasiljevic, P. Viterbo, J. Woollen, The ERA-40 re-analysis, Q. J. R. Meteorol. Soc. 131 (2005) 2961–3012, http://dx.doi.org/10.1256/qj.04.176.

[18] S. Musić, S. Nicković, 44-year wave hindcast for the Eastern Mediterranean, Coast. Eng. 55 (2008) 872–880, http://dx.doi.org/10.1016/j.coastaleng.2008.02.024.

[19] A.W. Ratsimandresey, M.G. Sotillo, J.C. Carretero Albiach, E. Álvarez Fanjul, H. Hajji, A 44-year high-resolution ocean and atmospheric hindcast for the Mediterranean Basin developed within the HIPOCAS Project, Coast. Eng. 55 (2008) 827–842, http://dx.doi.org/10.1016/j.coastaleng.2008.02.025.

[20] G. Besio, L. Mentaschi, A. Mazzino, Wave energy resource assessment in the Mediterranean Sea on the basis of a 35-year hindcast, Energy 94 (2016) 50–63, http://dx.doi.org/10.1016/j.energy.2015.10.044.

[21] U. Henfridsson, V. Neimane, K. Strand, R. Kapper, H. Bernhoff, O. Danielsson, M. Leijon, J. Sundberg, K. Thorburn, E. Ericsson, K. Bergman, Wave energy potential in the baltic sea and the danish part of The north sea, with reflections on the skagerrak, Renew. Energy 32 (2007) 2069–2084, http://dx.doi.org/10.1016/j.renene.2006.10.006.

[22] B. Aydoğan, B. Ayat, Y. Yüksel, Black Sea wave energy atlas from 13 years hindcasted wave data, Renew. Energy 57 (2013) 436–447, http://dx.doi.org/10.1016/j.renene.2013.01.047.

[23] L. Rusu, P. Pilar, C. Guedes Soares, Hindcast of the wave conditions along the west Iberian coast, Coast. Eng. 55 (2008) 906–919, http://dx.doi.org/10.1016/j.coastaleng.2008.02.029.

[24] M. Gonçalves, P. Martinho, C. Guedes Soares, Wave energy conditions in the western French coast, Renew. Energy 62 (2014) 155–163, http://dx.doi.org/10.1016/j.renene.2013.06.028.

[25] F. Fusco, G. Nolan, J.V. Ringwood, Variability reduction through optimal combination of wind/wave resources - an Irish case study, Energy 35 (2010) 314–325, http://dx.doi.org/10.1016/j.energy.2009.09.023.

[26] L. Cradden, H. Mouslim, O. Duperray, D. Ingram, Joint exploitation of wave and offshore wind power, Proc. Nineth Eur. Wave Tidal Energy Conf. (2011) 1–10.

[27] E.D. Stoutenburg, N. Jenkins, M.Z. Jacobson, Power output variations of co-located offshore wind turbines and wave energy converters in California, Renew. Energy 35 (2010) 2781–2791, http://dx.doi.org/10.1016/j.renene.2010.04.033.

[28] C. Pérez-Collazo, D. Greaves, G. Iglesias, A review of combined wave and offshore wind energy, Renew. Sustain. Energy Rev. 42 (2015) 141–153, http://dx.doi.org/10.1016/j.rser.2014.09.032.

[29] ORECCA, EU FP7 Co-ordinated Action Project “offshore Renewable Energy conversion—ORECCA”, 2012. http://www.orecca.eu/.

[30] MARINA Platform, EU FP7 Co-ordinated Action Project “marine Renewable Integrated Application Platform—MARINA Platform”, 2014, 2014, http://www.marina-platform.info/.

[31] G. Kallos, G. Galanis, C. Spyrou, C. Kalogeri, A. Adam, P. Athanasiadis, Offshore energy mapping for northeast Atlantic and Mediterranean: MARINA PLATFORM project, Geophys. Res. Abstr. 14 (2012) EGU2012–10767.

[32] TROPOS, EU FP7 Co-ordinated Action Project “modular Multi-use Deep Water Offshore Platform Harnessing and Servicing Mediterranean, Subtropical and Tropical Marine and Maritime Resources—TROPOS”, 2013. http://www.troposplatform.eu/.

[33] H2OCEAN, EU FP7 Co-ordinated Action Project “H2OCEAN”, 2014. http://www.h2ocean-project.eu/.

[34] MERMAID, EU FP7 Co-ordinated Action Project “innovative Multi-purpose Offshore Platforms: Planning, Design and Operation—MERMAID”, 2014. http://www.vliz.be/projects/mermaidproject/.

[35] X.G. Larsen, C. Kalogeri, G. Galanis, G. Kallos, A statistical methodology for the estimation of extreme wave conditions for offshore renewable applications, Renew. Energy 80 (2015) 205–218.

[36] P. Patlakas, G. Galanis, N. Barranger, G. Kallos, Extreme wind events in a complex maritime environment: ways of quantification, J. Wind Eng. Ind. Aerodyn. 149 (2016) 89–101, http://dx.doi.org/10.1016/j.jweia.2015.11.006.

[37] E.C. Edwards, L.C. Cradden, D.M. Ingram, C. Kalogeri, Verification within wave resource assessments. Part 1: statistical analysis, Int. J. Mar. Energy 8 (2015) 50–69.

[38] E.C. Edwards, L.C. Cradden, D.M. Ingram, C. Kalogeri, Verification within wave resource assessments. Part 2: systematic trends in the fit of spectral values, Int. J. Mar. Energy 8 (2014) 70–83.

[39] H. Dupuis, D. Michel, A. Sottolichio, Wave climate evolution in the Bay of Biscay over two decades, J. Mar. Syst. 63 (2006) 105–114, http://dx.doi.org/10.1016/j.jmarsys.2006.05.009.

[40] G. Dodet, X. Bertin, R. Taborda, Wave climate variability in the North-East Atlantic Ocean over the last six decades, Ocean. Model 31 (2010) 120–131, http://dx.doi.org/10.1016/j.ocemod.2009.10.010.

[41] E. Tyrlis, F.S. Tymvios, C. Giannakopoulos, J. Lelieveld, The role of blocking in the summer 2014 collapse of Etesians over the eastern Mediterranean, J. Geophys. Res. Atmos. 120 (2015) 6777–6792, http://dx.doi.org/10.1002/2015JD023543.

[42] U. Ulbrich, D. Belušić, J. Jacobeit, P. Knippertz, F.G. Kuglitsch, G.C. Leckebusch, J. Luterbacher, M. Maugeri, P. Maheras, K.M. Nissen, V. Pavan, J.G. Pinto, H. Saaroni, S. Seubert, A. Toreti, E. Xoplaki, B. Ziv, 5 – climate of the mediterranean: synoptic patterns, temperature, precipitation, winds, and their extremes, Clim. Mediterr. Reg. (2012) 301–346, http://dx.doi.org/10.1016/B978-0-12-416042-2.00005-7.

[43] G. Kallos, M. Astitha, P. Katsafados, C. Spyrou, Long-range transport of anthropogenically and naturally produced particulate matter in the Mediterranean and North Atlantic: current state of knowledge, J. Appl. Meteorol. Climatol. 46 (2007) 1230–1251, http://dx.doi.org/10.1175/JAM2530.1.

[44] E.B.L. Mackay, A.S. Bahaj, P.G. Challenor, Uncertainty in wave energy resource assessment. Part 2: variability and predictability, Renew. Energy 35 (2010) 1809–1819, http://dx.doi.org/10.1016/j.renene.2009.10.027.

[45] G. Kallos, The Regional weather forecasting system SKIRON, in: Proceedings, Symp. Reg. Weather Predict, Parallel Comput. Environ., Athens, Greece, 1997, p. 9.

[46] G. Kallos, A. Papadopoulos, P. Katsafados, S. Nickovic, Transatlantic Saharan dust transport: model simulation and results, J. Geophys. Res. 111 (2006), http://dx.doi.org/10.1029/2005jd006207.

[47] C. Spyrou, C. Mitsakou, G. Kallos, P. Louka, G. Vlastou, An improved limited area model for describing the dust cycle in the atmosphere, J. Geophys. Res. Atmos. 115 (2010) 1–19, http://dx.doi.org/10.1029/2009JD013682.

[48] P. Janssen, Chapter 3 ECMWF Wave Modeling and Satellite Altimeter Wave Data, 63, Elsevier Oceanogr. Ser., 2000, pp. 35–56, http://dx.doi.org/10.1016/S0422-9894(00)80004-5.

[49] Janssen Peter, The Interaction of Ocean Waves and Wind, Cambridge, University Press, 2004, http://dx.doi.org/10.1017/CBO9780511525018.

[50] G. Galanis, D. Hayes, G. Zodiatis, P.C. Chu, Y.H. Kuo, G. Kallos, Wave height characteristics in the Mediterranean sea by means of numerical modeling,

satellite data, statistical and geometrical techniques, Mar. Geophys Res. 33 (2012) 1–15.
[51] A. Papadopoulos, G. Kallos, P. Katsafados, S. Nickovic, The POSEIDON weather forecasting system: an overview, Glob. Atmos. Ocean. Syst. 8 (2002) 219–237.
[52] G. Emmanouil, G. Galanis, C. Kalogeri, G. Zodiatis, G. Kallos, 10-year high resolution study of wind, sea waves and wave energy assessment in the Greek offshore areas, Renew. Energy 90 (2016) 399–419, http://dx.doi.org/10.1016/j.renene.2016.01.031.
[53] C. Stathopoulos, A. Kaperoni, G. Galanis, G. Kallos, Wind power prediction based on numerical and statistical models, J. Wind Eng. Ind. Aerodyn. 112 (2013) 25–38.
[54] S.C. Albers, The LAPS wind analysis, Weather Forecsting 10 (1995) p342–352.
[55] J.R. Albers, S.C. McGinley, J.A. Birkenheuer, D.L. Smart, The local analysis and prediction system (LAPS): analyses of clouds, precipitation, and temperature, Weather Forecast 11 (1996) 273–287.
[56] J.R. Anderson, E.E. Hardy, J.T. Roach, R.E. Witmer, A Land Use and Land Cover Classification System for Use with Remote Sensor Data, USGS Prof. Pap. 964. 28 (1976).
[57] D.A. Miller, R.A. White, A conterminous United States multilayer soil characteristics dataset for regional climate and hydrology modeling, Earth Interact. 2 (1998) 2, http://dx.doi.org/10.1175/1087-3562 (1998).
[58] EMODNET. http://www.emodnet-physics.eu.
[59] D.S. Wilks, Statistical Methods in the Atmospheric Sciences, Academic Press, 1995, p. 467.
[60] F. Ardhuin, L. Bertotti, J.-R. Bidlot, L. Cavaleri, V. Filipetto, J.-M. Lefevre, P. Wittmann, Comparison of wind and wave measurements and models in the Western Mediterranean Sea, Ocean. Eng. 34 (2007) 526–541, http://dx.doi.org/10.1016/j.oceaneng.2006.02.008.
[61] A.W. Ratsimandresy, M.G. Sotillo, J.C. Carretero Albiach, E. Álvarez Fanjul, H. Hajji, A 44-year high-resolution ocean and atmospheric hindcast for the Mediterranean Basin developed within the HIPOCAS Project, Coast. Eng. 55 (2008) 827–842, http://dx.doi.org/10.1016/j.coastaleng.2008.02.025.
[62] B. Geyer, R. Weisse, P. Bisling, J. Winterfeldt, Climatology of North Sea wind energy derived from a model hindcast for 1958–2012, J. Wind Eng. Ind. Aerodyn. 147 (2015) 18–29, http://dx.doi.org/10.1016/j.jweia.2015.09.005.
[63] T. Lorenz, I. Barstad, A dynamical downscaling of ERA-Interim in the North Sea using WRF with a 3km grid-for wind resource applications, Wind Energy (2016), http://dx.doi.org/10.1002/we.1961.
[64] M.G. Sotillo, R. Aznar, F. Valero, The 44-year Mediterranean HIPOCAS wind database: a useful tool to analyse offshore extreme wind events from a long-term regional perspective, Coast. Eng. 55 (2008) 930–943, http://dx.doi.org/10.1016/j.coastaleng.2008.02.008.
[65] S. Abdalla, Effect of wind variability and variable air density on wave modeling, J. Geophys. Res. 107 (2002) 326–329, http://dx.doi.org/10.1029/2000JC000639.
[66] I. Troen, E. Lundtang Petersen, European Wind Atlas, Risø National Laboratory, 1989.
[67] E. Rusu, Evaluation of the wave energy conversion efficiency in various coastal environments, Energies 7 (2014) 4002–4018, http://dx.doi.org/10.3390/en7064002.
[68] J.P. Kofoed, P. Frigaard, E. Friis-Madsen, H.C. Sørensen, Prototype testing of the wave energy converter wave dragon, Renew. Energy 31 (2006) 181–189, http://dx.doi.org/10.1016/j.renene.2005.09.005.